

# Chapter

## 2

# *Gravity Methods*

### 2.1. INTRODUCTION

#### 2.1.1. General

Gravity prospecting involves measurements of variations in the gravitational field of the earth. One hopes to locate local masses of greater or lesser density than the surrounding formations and learn something about them from the irregularities in the earth's field. It is not possible, however, to determine a unique source for an observed anomaly. Observations normally are made at the earth's surface, but underground surveys also are carried out occasionally.

Gravity prospecting is used as a reconnaissance tool in oil exploration; although expensive, it is still considerably cheaper than seismic prospecting. Gravity data are also used to provide constraints in seismic interpretation. In mineral exploration, gravity prospecting usually has been employed as a secondary method, although it is used for detailed follow-up of magnetic and electromagnetic anomalies during integrated base-metal surveys. Gravity surveys are sometimes used in engineering (Arzi, 1975) and archaeological studies.

Like magnetics, radioactivity, and some electrical techniques, gravity is a natural-source method. Local variations in the densities of rocks near the surface cause minute changes in the gravity field. Gravity and magnetics techniques often are grouped together as the *potential methods*, but there are basic differences between them. Gravity is an inherent property of mass, whereas the magnetic state of matter depends on other factors, such as the inducing fields and/or the orientations of magnetic domains. Density variations are relatively small, and the gravity effects of local masses are very small compared with the effect of the background field of the Earth as a whole (often of the order of 1 part in  $10^6$  to  $10^7$ ), whereas magnetic anomalies often are large relative to the main field. The time variation of the magnetic field is complex, whereas the gravity field is constant (ignoring "earth tides"). Corrections to gravity read-

ings are more complicated and more important than in magnetic or other geophysical methods. Gravity field operations are more expensive than magnetic operations, and field work is slower and requires more highly skilled personnel.

#### 2.1.2. History of Gravity Exploration

Galileo Galilei, in about 1589, so legend tells us, dropped light and heavy weights from the Leaning Tower of Pisa in an attempt to determine how weight affects the speed at which a given object falls. Johann Kepler worked out the laws of planetary motion, and this enabled Sir Isaac Newton to discover the universal law of gravitation (*Mathematical Principles of Natural Philosophy*, 1685-87).

The expeditions of the French Academy of Sciences to Lapland and Peru (Ecuador) in 1735-45 gave Pierre Bouguer the opportunity to establish many of the basic gravitational relationships, including variations of gravity with elevation and latitude, the horizontal attraction due to mountains, and the density of the Earth.

Captain Henry Kater, in 1817, introduced the compound pendulum, with interchangeable centers of oscillation and suspension, which became the major tool for gravity investigation for over a century. Because the variations in gravitational attraction are so small, Baron Roland von Eötvös set out to measure derivatives rather than total magnitudes. He completed his first torsion balance (a modification of the Coulomb balance) in 1890 and made the first gravity survey on the ice of Lake Balaton in 1901. F. A. Vening Meinesz, in 1923, measured gravity with pendulums on board a Dutch submarine and demonstrated gravity variations over various areas of the oceans, especially the large gravity effects near the Indonesian trench.

In December 1922, a torsion-balance survey of the Spindletop oil field initiated geophysical exploration for oil. In late 1924, a test well on the Nash salt dome in Brazoria County, Texas, verified the

gravity interpretation, becoming the first geophysical hydrocarbon discovery, although the first producing oil well did not come in until January 1926.

The last half of the 1920s saw extensive gravity surveys with the torsion balance. In 1929 the portable pendulum began to be used, followed in 1932 by the stable gravimeter (and the unstable gravimeter, which was not publicly described until 1937). By 1940, gravimeters had become so stable and convenient that torsion balances and portable pendulums disappeared from use. LaCoste (1934) described the zero-length spring, but the first workable LaCoste gravimeter did not appear until 1939. In subsequent years, gravimeters have been adapted (LaFehr, 1980) to measurements under water, on moving ships and aircraft, and in boreholes.

The major addition to our knowledge of gravity in recent years has come from observations of satellite paths (Kahn, 1983). These have considerably increased our knowledge of the detailed shape of the Earth, but this has not changed gravity exploration significantly.

In the 1940s, graphic and grid methods of isolating anomalies were developed, and the anomalies that result from simple shapes were calculated. The computing power made available by digital computers since the 1960s has considerably increased our interpretation capabilities, the ultimate goal being solution of the *inverse problem* (§2.7.9).

## 2.2. PRINCIPLES OF GRAVITY

### 2.2.1. Newton's Law of Gravitation

The force of gravitation is expressed by *Newton's law*: The force between two particles of masses  $m_1$  and  $m_2$  is directly proportional to the product of the masses and inversely proportional to the square of the distance between the centers of mass:

$$\mathbf{F} = \gamma(m_1 m_2 / r^2) \mathbf{r}_1 \quad (2.1)$$

where  $\mathbf{F}$  is the force on  $m_2$ ,  $\mathbf{r}_1$  is a unit vector directed from  $m_2$  toward  $m_1$ ,  $r$  is the distance between  $m_1$  and  $m_2$ , and  $\gamma$  is the universal gravitational constant. Note that the force  $\mathbf{F}$  is always attractive. In SI units the value of  $\gamma$  is  $6.672 \times 10^{-11}$  N m<sup>2</sup>/kg<sup>2</sup> or in cgs units  $6.672 \times 10^{-8}$  dyne cm<sup>2</sup>/g<sup>2</sup>.

### 2.2.2. Acceleration of Gravity

The acceleration of  $m_2$  due to the presence of  $m_1$  can be found by dividing  $\mathbf{F}$  by  $m_2$  in Equation (2.1), that is,

$$\mathbf{g} = (\gamma m_1 / r^2) \mathbf{r}_1 \quad (2.2a)$$

The acceleration  $\mathbf{g}$  is equal to the gravitational force per unit mass due to  $m_1$ . If  $m_1$  is the mass of the Earth,  $M_e$ ,  $\mathbf{g}$  becomes the *acceleration of gravity* and is given by

$$\mathbf{g} = (\gamma M_e / R_e^2) \mathbf{r}_1 \quad (2.2b)$$

$R_e$  being the radius of the Earth and  $\mathbf{r}_1$  extending downward toward the center of the Earth. (It is customary to use the same symbol  $\mathbf{g}$  whether it is due to the Earth or a mass  $m$ .) The acceleration of gravity was first measured by Galileo in his famous experiment at Pisa. The numerical value of  $\mathbf{g}$  at the Earth's surface is about 980 cm/s<sup>2</sup>. In honor of Galileo, the unit of acceleration of gravity, 1 cm/s<sup>2</sup>, is called the galileo or Gal.

Gravimeters used in field measurements have a sensitivity of about  $10^{-5}$  Gal or 0.01 mGal, although the reading accuracy is generally only 0.03 to 0.06 mGal. As a result, they are capable of distinguishing changes in the value of  $\mathbf{g}$  with a precision of one part in  $10^8$ . Microgravimeters are available with measuring accuracy of about 5  $\mu$ Gal.

### 2.2.3. Gravitational Potential

(a) *Newtonian or three-dimensional potential*. Gravitational fields are conservative; that is, the work done in moving a mass in a gravitational field is independent of the path traversed and depends only on the end points (§A.3.4). If the mass is eventually returned to its original position, the net energy expenditure is zero, regardless of the path followed. Another way of expressing this is to say that the sum of kinetic (motion) energy and potential (position) energy is constant within a closed system.

The gravitational force is a vector whose direction is along the line joining the centers of the two masses. The force giving rise to a conservative field may be derived from a scalar potential function  $U(x, y, z)$ , called the *Newtonian or three-dimensional potential*, by finding the gradient [Eqs. (A.17), (A.30), and (A.31)]:

$$\begin{aligned} \nabla U(x, y, z) &= -\mathbf{F}(x, y, z)/m_2 \\ &= -\mathbf{g}(x, y, z) \end{aligned} \quad (2.3a)$$

In spherical coordinates (Fig. A.4b) this becomes

$$\begin{aligned} \nabla U(r, \theta, \phi) &= -\mathbf{F}(r, \theta, \phi)/m_2 \\ &= -\mathbf{g}(r, \theta, \phi) \end{aligned} \quad (2.3b)$$

Alternatively, we can solve this equation for the

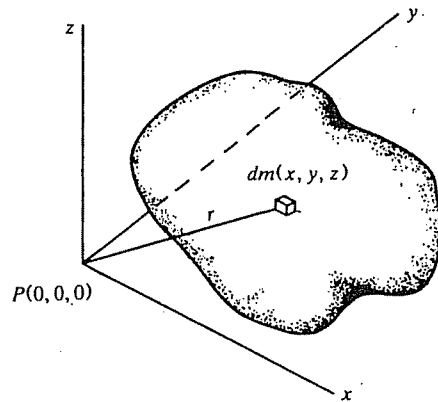


Figure 2.1. Potential of three-dimensional mass.

gravitational potential in the form [Eq. (A.16)]

$$\begin{aligned} U(r, \theta, \phi) &= \int_{\infty}^r (\nabla U) \cdot dr \\ &= - \int_{\infty}^r \mathbf{g} \cdot dr \end{aligned} \quad (2.4)$$

which is a statement of the work done in moving a unit mass from infinity (that is, a very distant point), by any path, to a point distant  $r$  from the point mass producing the gravitational field. Using Equation (2.2a) in scalar form, we get

$$U(r) = -\gamma \int_{\infty}^r m(1/r^2) dr = \gamma m/r \quad (2.5)$$

It is often simpler to solve gravity problems by calculating the scalar potential  $U$  rather than the vector  $\mathbf{g}$  and then to obtain  $\mathbf{g}$  from Equation (2.3).

Considering a three-dimensional mass of arbitrary shape as in Figure 2.1, the potential and acceleration of gravity at a point outside the mass can be found by dividing the mass into small elements and integrating to get the total effect. From Equation (2.5), the potential due to an element of mass  $dm$  at the point  $(x, y, z)$  a distance  $r$  from  $P(0, 0, 0)$  is

$$dU = \gamma dm/r = \gamma \rho dx dy dz/r$$

where  $\rho(x, y, z)$  is the density, and  $r^2 = x^2 + y^2 + z^2$ . Then the potential of the total mass  $m$  is

$$U = \gamma \int_x \int_y \int_z (\rho/r) dx dy dz \quad (2.6a)$$

Because  $\mathbf{g}$  is the acceleration of gravity in the  $z$  direction (positive vertically downward), and assuming  $\rho$  constant,

$$g = -(\partial U / \partial z)$$

$$= \gamma \rho \int_x \int_y \int_z (z/r^3) dx dy dz \quad (2.7a)$$

Sometimes it is more convenient to use cylindrical coordinates (Figure A.4a). Because  $dx dy dz = r_0 dr_0 d\theta dz$  and  $r^2 = r_0^2 + z^2$ ,  $r_0^2 = x^2 + y^2$ , the potential becomes

$$U = \gamma \rho \int_{r_0} \int_{\theta} \int_z (r_0/r) dr_0 d\theta dz \quad (2.6b)$$

and the acceleration in the  $z$  direction is

$$g = \gamma \rho \int_{r_0} \int_{\theta} \int_z (r_0 z/r^3) dr_0 d\theta dz \quad (2.7b)$$

In spherical coordinates,

$$dx dy dz = r^2 \sin \theta dr d\theta d\phi$$

hence,

$$U = \gamma \rho \int_r \int_{\theta} \int_{\phi} r \sin \theta dr d\theta d\phi \quad (2.6c)$$

Taking the  $z$  axis along the polar axis,

$$\begin{aligned} g &= -\partial U / \partial z \\ &= -\gamma \rho \int_r \int_{\theta} \int_{\phi} (z/r) \sin \theta dr d\theta d\phi \\ &= -\gamma \rho \int_r \int_{\theta} \int_{\phi} \sin \theta \cos \theta dr d\theta d\phi \end{aligned} \quad (2.7c)$$

because  $z/r = \cos \theta$ . (The minus sign indicates that  $\mathbf{g}$  is directed toward the mass  $dm$  at the center of the sphere.)

(b) *Logarithmic or two-dimensional potential.* If the mass is very long in the  $y$  direction and has a uniform cross section of arbitrary shape in the  $xz$  plane, the gravity attraction derives from a logarithmic (rather than Newtonian) potential. Then Equation (2.6a) becomes

$$U = \gamma \rho \int_x \int_z dx dz \int_{-\infty}^{\infty} (1/r) dy$$

With some manipulation (see problem 1), the logarithmic potential becomes

$$U = 2\gamma \rho \int_x \int_z \ln(1/r') dx dz \quad (2.8)$$

where  $r'^2 = x^2 + z^2$ . The gravity effect for the two-dimensional body is

$$g = -\partial U / \partial z = 2\gamma \int_x \int_z \rho(z/r'^2) dx dz \quad (2.9)$$

### 2.2.4. Potential-Field Equations

The divergence theorem [Gauss's theorem; Eq. (A.27)] states that the integral of the divergence of a vector field  $\mathbf{g}$  over a region of space  $V$  is equivalent to the integral of the outward normal component of the field  $\mathbf{g}$  over the surface enclosing the region. We have

$$\int_V \nabla \cdot \mathbf{g} dv = \int_S g_n ds \quad (2.10)$$

If there is no attracting matter within the volume, the integrals are zero and  $\nabla \cdot \mathbf{g} = 0$ . But from Equation (2.3a) the gravitational force is the gradient of the scalar potential  $U$ , so that

$$-\nabla \cdot \mathbf{g} = \nabla \cdot \nabla U = \nabla^2 U = 0 \quad (2.11a)$$

that is, the potential in free space satisfies Laplace's equation. In cartesian coordinates, Laplace's equation is

$$\nabla^2 U = \frac{\partial^2 U}{\partial x^2} + \frac{\partial^2 U}{\partial y^2} + \frac{\partial^2 U}{\partial z^2} = 0 \quad (2.11b)$$

[see Eq. (A.37) for Laplace's equation in spherical coordinates]. Also, because  $\mathbf{g} = -\partial U / \partial \mathbf{z}$ , and any derivative of a solution of a differential equation is also a solution, we have

$$\nabla^2 \mathbf{g} = 0 \quad (2.11c)$$

If, on the other hand, there is a particle of mass at the center of a sphere of radius  $r$ , then

$$\begin{aligned} \int_S g_n ds &= -(\gamma m/r^2)(4\pi r^2) \\ &= -4\pi\gamma m \end{aligned} \quad (2.12a)$$

the minus meaning that  $g_n$  is opposite to  $\mathbf{n}$ , the outward-drawn normal. It can be shown (see problem 2) that this result holds regardless of the shape of the surface and the position and size of the mass within the surface. If the surface encloses several masses of total mass  $M$ , we can write

$$\int_V \nabla \cdot \mathbf{g} dv = \int_S g_n ds = -4\pi\gamma M \quad (2.12b)$$

If the volume  $V$  is very small, enclosing only a point, we can remove the integral sign to give

$$\nabla \cdot \mathbf{g} = -4\pi\gamma\rho \quad (2.13a)$$

where  $\rho$  is the density at the point. Then, from

Equation (2.3a),

$$\nabla^2 U = 4\pi\gamma\rho \quad (2.13b)$$

which is *Poisson's equation*.

Equations (2.11a) and (2.13b) state that the gravity potential satisfies Laplace's equation in free space and Poisson's equation in a region containing mass.

These equations imply that various distributions of mass can produce the same potential field over a surface (Skeels, 1947); this is sometimes called the "inherent ambiguity" of gravity interpretation. Sometimes it is convenient to substitute for masses distributed throughout a volume  $V$  a fictitious *surface density* of mass over a surface  $S$  enclosing  $V$  such that the effect outside  $S$  is the same. From Equations (2.12b) and (2.13a) we have

$$\int_V (-4\pi\gamma\rho) dv = \int_S g_n ds \quad (2.14)$$

that is, the component of gravity perpendicular to the surface gives the equivalent surface density. For an equipotential surface, this is merely the total gravitational field.

### 2.2.5. Derivatives of the Potential

Quantities useful in gravity analysis may be obtained by differentiating the potential in various ways. We have already noted in Equation (2.7a) that vertical gravity  $g = -\partial U / \partial z$ . This is the quantity measured by gravimeters.

The first vertical derivative of  $g$  [from Eq. (2.7a)] is

$$\begin{aligned} \partial g / \partial z &= -\partial^2 U / \partial z^2 \\ &= -U_{zz} \\ &= \gamma\rho \int_x \int_y \int_z (1/r^3 - 3z^2/r^5) dx dy dz \end{aligned} \quad (2.15)$$

where subscripts indicate derivatives of  $U$ . Measurements occasionally are made of the vertical gradient (Falkiewicz, 1976; Jordan, 1978; Ager and Lilard, 1982; Butler, 1984).

The second vertical derivative is

$$\begin{aligned} \partial^2 g / \partial z^2 &= -\partial^3 U / \partial z^3 \\ &= -U_{zzz} \\ &= 3\gamma\rho \int_x \int_y \int_z (5z^3/r^7 - 3z/r^5) dx dy dz \end{aligned} \quad (2.16)$$

This derivative frequently is employed in gravity interpretation for isolating anomalies (§2.6.5) and for upward and downward continuation (§2.6.7).

Derivatives tend to magnify near-surface features by increasing the power of the linear dimension in the denominator. That is, because the gravity effect varies inversely as the distance squared, the first and second derivatives vary as the inverse of the third and fourth powers, respectively (for three-dimensional bodies).

By taking the derivatives of  $g$  in Equation (2.7a) along the  $x$  and  $y$  axes, we obtain the components of the *horizontal gradient of gravity*:

$$\begin{aligned} U_{xz} &= -\partial g / \partial x \\ &= 3\gamma\rho \int_x \int_y \int_z (xz/r^5) dx dy dz \quad (2.17) \end{aligned}$$

and similarly for the  $y$  component  $U_{yz}$ . The horizontal gradient can be determined from gravity profiles or map contours as the slope or rate of change of  $g$  with horizontal displacement. The horizontal gradient is useful in defining the edges and depths of bodies (Stanley, 1977).

The *differential curvature* (or *horizontal directive tendency*, HDT) is a measure of the warped or curved shape of the potential surface. From Equation (2.6a),

$$U_{xx} = \gamma\rho \int_x \int_y \int_z (3x^2/r^5 - 1/r^3) dx dy dz \quad (2.18)$$

Other components are  $U_{yy}$  and  $U_{xy}$ . The differential curvature (HDT) is given by

$$\begin{aligned} \text{HDT} &= \left\{ (U_{yy} - U_{xx})^2 + (2U_{xy})^2 \right\}^{1/2} \\ &= 3\gamma\rho \int_x \int_y \int_z \left\{ (x^2 + y^2)/r^5 \right\} dx dy dz \quad (2.19) \end{aligned}$$

It is not possible to measure  $U_{xx}$ ,  $U_{yy}$ ,  $U_{xy}$ , or HDT directly. Differential curvature can be obtained from torsion-balance measurements.

## 2.3. GRAVITY OF THE EARTH

### 2.3.1. Figure of the Earth

(a) *General*. Gravity prospecting evolved from the study of the Earth's gravitational field, a subject of interest to geodesists for determining the shape of the Earth. Because the Earth is not a perfect homogeneous sphere, gravitational acceleration is not constant over the Earth's surface.

The magnitude of gravity depends on five factors: latitude, elevation, topography of the surrounding terrain, earth tides, and density variations in the subsurface. Gravity exploration is concerned with

anomalies due to the last factor, and these anomalies generally are much smaller than the changes due to latitude and elevation, although larger than the anomalies due to tidal and (usually) topographic effects. The change in gravity from equatorial to polar regions amounts to about 5 Gal, or 0.5% of the average value of  $g$  (980 Gal), and the effect of elevation can be as large as 0.1 Gal, or 0.01% of  $g$ . A gravity anomaly considered large in oil exploration, on the other hand, would be 10 mGal, or 0.001% of  $g$ , whereas in mineral exploration a large anomaly would be 1 mGal. Thus, variations in  $g$  that are significant in prospecting are small in comparison with the magnitude of  $g$  and also in comparison with latitude and elevation effects. Fortunately, we can, with good accuracy, remove most of the effects of factors that are not of interest in prospecting.

(b) *The reference spheroid*. The shape of the Earth, determined by geodetic measurements and satellite tracking, is nearly spheroidal, bulging at the equator and flattened at the poles. The *polar flattening* is  $(R_{eq} - R_p)/R_{eq} = 1/298.25$ , where  $R_{eq}$  and  $R_p$  are the Earth's equatorial and polar radii, respectively.

The *reference spheroid* is an oblate ellipsoid that approximates the mean sea-level surface (*geoid*), with the land above it removed. In 1930 the International Union of Geodesy and Geophysics adopted a formula (Nettleton, 1976, p. 17) for the theoretical value of gravity  $g_t$ , but this has been superseded (Woolard, 1979) by the Geodetic Reference System 1967 (GRS67):

$$\begin{aligned} g_t &= 978,031.846(1 + 0.005,278,895 \sin^2 \phi \\ &\quad + 0.000,023,462 \sin^4 \phi) \text{ mGal} \quad (2.20) \end{aligned}$$

where  $\phi$  is latitude.

(c) *The geoid*. Mean continental elevations are about 500 m, and maximum land elevations and ocean depressions are of the order of 9,000 m referred to sea level. Sea level is influenced by these variations and other lateral density changes. We define mean sea level (the equipotential for the Earth's gravity plus centrifugal effects), called the *geoid*, as the average sea level over the oceans and over the surface of sea water that would lie in canals if they were cut through the land masses.

The simplified *figure of the Earth* allows for increasing density with depth, but not for lateral variations, which are the objects of gravity exploration. Because of the lateral variations, the geoid and reference spheroid do not coincide. Local mass anomalies warp the geoid as in Figure 2.2a. We might expect

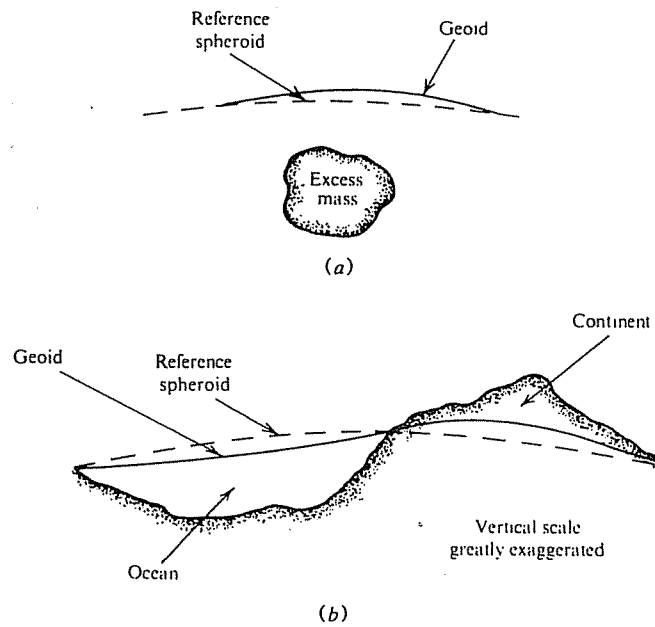


Figure 2.2. Comparison of reference spheroid and geoid. (a) Warping of the geoid by a local mass. (b) Large-scale warping.

the geoid to be warped upward under the continents because of attracting material above, and downward over the ocean basins because of the low density of water (Figure 2.2b). However, deviations from the spheroid do not correlate with the continents nor with the lithospheric plates, suggesting that density differences exist below the lithosphere. The deviations between the two surfaces (Kahn, 1983) are as much as 100 m.

### 2.3.2. Gravity Reduction

(a) *General.* Gravity readings are generally influenced by the five factors listed in Section 2.3.1a, hence we must make corrections to reduce gravity readings to the values they would have on a datum equipotential surface such as the geoid (or a surface everywhere parallel to it).

(b) *Latitude correction.* Both the rotation of the Earth and its equatorial bulge produce an increase of gravity with latitude. The centrifugal acceleration due to the rotating Earth is maximum at the equator and zero at the poles; it opposes the gravitational acceleration, while the polar flattening increases gravity at the poles by making the geoid closer to the Earth's center of mass. The latter effect is counteracted partly by the increased attracting mass at the equator. A *latitude correction*  $\Delta g_L$  is obtained by

differentiating Equation (2.20):

$$\begin{aligned} \Delta g_L / \Delta s &= (1/R_e) \Delta g_i / \Delta \phi \\ &= 0.811 \sin 2\phi \text{ mGal/km} \quad (2.21a) \end{aligned}$$

$$= 1.305 \sin 2\phi \text{ mGal/mile} \quad (2.21b)$$

where  $\Delta s = N-S$  horizontal distance =  $R_e \Delta \phi$  and  $R_e$  is the radius of the Earth ( $\approx 6368$  km). The correction is a maximum at latitude  $45^\circ$  where it amounts to  $0.01$  mGal/(13 m) and it is zero at the equator and poles. The correction is added to  $g$  as we move toward the equator.

(c) *Free-air correction.* Since gravity varies inversely with the square of distance, it is necessary to correct for changes in elevation between stations to reduce field readings to a datum surface. The *free air correction* does not take account of the material between the station and the datum plane. It is obtained by differentiating the scalar equation equivalent to Equation (2.2b); the result is (dropping the minus sign)

$$\begin{aligned} \Delta g_{FA} / \Delta R &= 2\gamma M_e / R_e^3 = 2g / R_e \\ &= 0.3086 \text{ mGal/m} \quad (2.22a) \end{aligned}$$

$$= 0.09406 \text{ mGal/ft} \quad (2.22b)$$

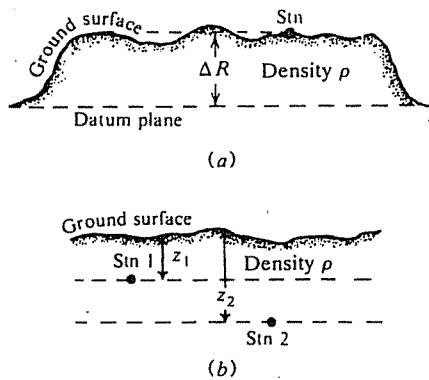


Figure 2.3. Bouguer correction. (a) Station on a broad plateau. (b) Underground stations.

at 45° latitude. The free-air correction is added to the field reading when the station is above the datum plane and subtracted when below it.

To make latitude and free-air corrections, station position must be known precisely. For an accuracy of 0.01 mGal, the usual accuracy of the gravimeter, N-S location (at 45° latitude) must be known to within 13 m (40 ft) and elevation to 3 cm (1 in.).

(d) *Bouguer correction.* The *Bouguer correction* accounts for the attraction of material between the station and datum plane that was ignored in the free-air calculation. If the station were centrally located on a plateau of large horizontal extent and uniform thickness and density (Fig. 2.3a), the gravity reading would be increased by the attraction of this slab between the station and the datum. The Bouguer correction is given by

$$\Delta g_B/\Delta R = 2\pi\gamma\rho \\ = 0.04192\rho \text{ mGal/m} \quad (2.23a)$$

$$= 0.01278\rho \text{ mGal/ft} \quad (2.23b)$$

where  $\rho$  is the slab density in grams per cubic centimeter [see Eq. (2.57)]. If we assume an average density for crustal rocks of 2.67 g/cm<sup>3</sup>, the numerical value is

$$\Delta g_B/\Delta R = 0.112 \text{ mGal/m} \quad (2.24a)$$

$$= 0.0341 \text{ mGal/ft} \quad (2.24b)$$

The Bouguer correction is applied in the opposite sense to free air, that is, it is subtracted when the station is above the datum and vice versa.

When gravity measurements are made at underground stations, as in Figure 2.3b, the slab between stations at depths  $z_1$  and  $z_2$  exerts an attraction downward on station 1 and upward on 2. Thus the difference in gravity between them is  $4\pi\gamma\rho(z_2 - z_1)$  mGal, that is, the Bouguer correction is doubled.

The Bouguer and free-air corrections are often combined into an *elevation correction*. From Equations (2.22) and (2.23) the result is

$$\begin{aligned} \Delta g_E/\Delta R &= \Delta g_{FA}/\Delta R - \Delta g_B/\Delta R \\ &\stackrel{FM}{=} BC \\ &= (0.3086 - 0.0419\rho) \text{ mGal/m} \quad (2.25a) \end{aligned}$$

$$= (0.0941 - 0.0128\rho) \text{ mGal/ft} \quad (2.25b)$$

The elevation correction is applied in the same way as the free-air correction.

Two assumptions were made in deriving the Bouguer correction: (1) The slab is of uniform density and (2) it is of infinite horizontal extent; neither is really valid. To modify the first, one needs considerable knowledge of local rock types and densities. The second is taken care of in the next reduction.

(e) *Terrain correction.* The terrain correction allows for surface irregularities in the vicinity of the station. Hills above the elevation of the gravity station exert an upward pull on the gravimeter, whereas valleys (lack of material) below it fail to pull downward on it. Thus both types of topographic undulations affect gravity measurements in the same sense and the *terrain correction* is added to the station reading.

There are several methods for calculating terrain corrections, all of which require detailed knowledge of relief near the station and a good topographical map (contour interval ~ 10 m or 50 ft or smaller) extending considerably beyond the survey area. The usual procedure is to divide the area into compartments and compare the elevation within each compartment with the station elevation. This can be done by outlining the compartments on a transparent sheet overlying a topographic map. The most common template used concentric circles and radial lines, making sectors whose areas increased with distance from the station. The gravity effect of a single sector was calculated from the following for-

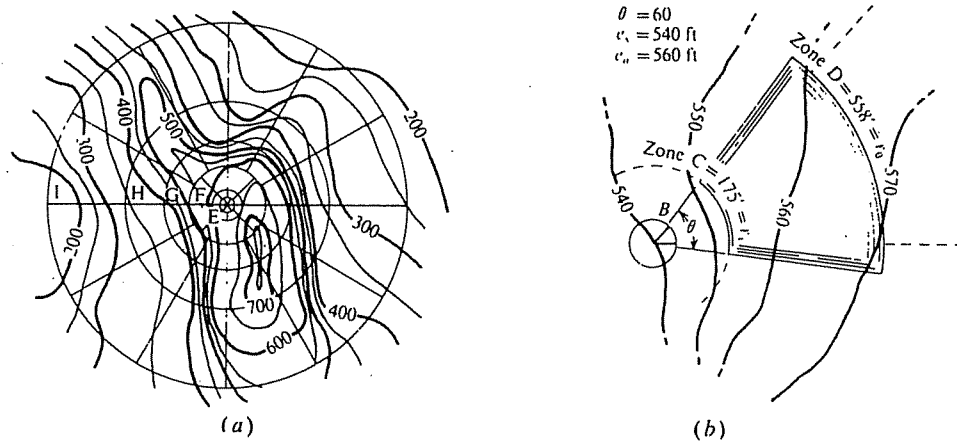


Figure 2.4. Use of terrain chart with topographic map. (a) Terrain chart overlying map. (b) Enlarged view of a single zone.

mula [Eq. (2.58)]:

$$\delta g_T(r, \theta) = \gamma \rho \theta \left\{ (r_o - r_i) + (r_i^2 + \Delta z^2)^{1/2} - (r_o^2 + \Delta z^2)^{1/2} \right\} \quad (2.26)$$

where  $\theta$  is the sector angle (radians),  $\Delta z = |z_s - z_a|$ ,  $z_s$  is the station elevation,  $z_a$  is the average elevation in the sector, and  $r_o$  and  $r_i$  are the outer and inner sector radii. The terrain correction  $\Delta g_T$  is the sum of the contributions of all sectors:

$$\Delta g_T = \sum_r \sum_\theta \delta g_T(r, \theta) \quad (2.27)$$

The use of a terrain chart of this type is illustrated in Figure 2.4. The transparent template is placed over the topographic map with the center of the circles at the gravity station. The average elevation within a single compartment is estimated from the contours within it and subtracted from the known station elevation. The difference is  $\Delta z$  in Equation (2.26), from which the contribution to  $\Delta g_T$  is calculated for the compartment. Tables of terrain corrections such as Table 2.1 facilitated this operation. [Hammer (1982) gives corrections for subdivisions of the inner zones required in microgravity surveys for engineering and archaeological surveys.] Note that there was no provision for relief within 2 m of the station, that is, it has to be flat for a 2 m distance from the station. It can be seen from Table 2.1 that the correction is small if  $r > 20z$ ,  $r$  being the average distance from the compartment to the station.

Other methods for segmenting the topographic map occasionally were applied; for instance, when contours were practically linear, there was no advantage in using circular sectors. An alternative scheme

used elementary areas so proportioned that the gravity effect of each was the same regardless of distance.

Terrain corrections for outer zones are often made on a computer using elevations on a regular grid (Krohn, 1976). Regardless of the approach, the topographic reduction is a slow and tedious task. Furthermore, in areas of steep and erratic slopes, it usually is not very accurate, particularly for relief in the vicinity of the station itself. At the edge of a steep cliff or gorge, the terrain correction is almost inevitably in error. A better solution is to move the gravity station away from sharp relief features if this is possible.

Bouguer anomalies (§2.3.2h) for marine surface and airborne surveys require a different terrain correction from that discussed earlier. The Bouguer correction is calculated (for marine data) as if the water depth were everywhere constant, and hence it is discontinuous over abrupt elevation changes. The terrain correction is made discontinuous to compensate for the Bouguer correction discontinuities. To the left of a two-dimensional vertical step in the sea floor (Fig. 2.5), the terrain correction is positive due to the deeper water on the right (analogous to a nearby valley in land work), and it is negative to the right of the step.

(f) Earth-tide correction. Instruments for measuring gravity are sensitive enough to record the changes in  $g$  caused by movement of the Sun and Moon, changes that depend on latitude and time. Their range is about 0.3 mGal. Figure 2.6 shows calculated and measured tidal variations for a stationary gravimeter.

The correction can be calculated from knowledge of the locations of the Sun and Moon. However, because the variation is smooth and relatively slow,

Table 2.1. Terrain corrections.

Zone B		Zone C		Zone D		Zone E		Zone F		Zone G		Zone H		Zone I	
4 sectors		6 sectors		6 sectors		8 sectors		8 sectors		12 sectors		12 sectors		12 sectors	
54.6' - 54.6'		54.6' - 54.6'		54.6' - 55.8'		55.8' - 1280'		55.8' - 1280'		2936' - 5018'		2936' - 5018'		5018' - 8578'	
$\pm z$	$d\theta_T$														
0.0 - 1.1	0.00000	0.0 - 4.3	0.00000	0.0 - 7.7	0.00000	-0.18	0.00000	-0.27	0.00000	-0.58	0.00000	-0.75	0.00000	-0.99	0.00000
1.1 - 1.9	0.00133	4.3 - 7.5	0.00133	7.7 - 13.4	0.00133	18 - 30	0.00133	27 - 46	0.00133	58 - 100	0.00133	75 - 131	0.00133	99 - 171	0.00133
1.9 - 2.5	0.00267	7.5 - 9.7	0.00267	13.4 - 17.3	0.00267	30 - 39	0.00267	46 - 60	0.00267	100 - 129	0.00267	131 - 169	0.00267	171 - 220	0.00267
2.5 - 2.9	0.0040	9.7 - 11.5	0.0040	17.3 - 20.5	0.0040	39 - 47	0.0040	60 - 71	0.0040	129 - 153	0.0040	169 - 200	0.0040	220 - 261	0.0040
2.9 - 3.4	0.0053	11.5 - 13.1	0.0053	20.5 - 23.2	0.0053	47 - 53	0.0053	71 - 80	0.0053	153 - 173	0.0053	200 - 226	0.0053	261 - 296	0.0053
3.4 - 3.7	0.0067	13.1 - 14.5	0.0067	23.2 - 25.7	0.0067	53 - 58	0.0067	80 - 88	0.0067	173 - 191	0.0067	226 - 250	0.0067	296 - 327	0.0067
3.7 - 7	0.0133	14.5 - 24	0.0133	25.7 - 43	0.0133	58 - 97	0.0133	88 - 146	0.0133	191 - 317	0.0133	250 - 414	0.0133	327 - 540	0.0133
7 - 9	0.0267	24 - 32	0.0267	43 - 56	0.0267	97 - 126	0.0267	146 - 189	0.0267	317 - 410	0.0267	414 - 535	0.0267	540 - 698	0.0267
9 - 12	0.040	32 - 39	0.040	56 - 66	0.040	126 - 148	0.040	189 - 224	0.040	410 - 486	0.040	535 - 633	0.040	698 - 827	0.040
12 - 14	0.053	39 - 45	0.053	66 - 76	0.053	148 - 170	0.053	224 - 255	0.053	486 - 552	0.053	633 - 719	0.053	827 - 938	0.053
14 - 16	0.067	45 - 51	0.067	76 - 84	0.067	170 - 189	0.067	255 - 282	0.067	552 - 611	0.067	719 - 796	0.067	938 - 1038	0.067
16 - 19	0.080	51 - 57	0.080	84 - 92	0.080	189 - 206	0.080	282 - 308	0.080	611 - 666	0.080	796 - 866	0.080	1038 - 1129	0.080
19 - 21	0.0935	57 - 63	0.0935	92 - 100	0.0935	206 - 222	0.0935	308 - 331	0.0935	666 - 716	0.0935	866 - 931	0.0935		
21 - 24	0.107	63 - 68	0.107	100 - 107	0.107	222 - 238	0.107	331 - 353	0.107	716 - 764	0.107	931 - 992	0.107		
24 - 27	0.120	68 - 74	0.120	107 - 114	0.120	238 - 252	0.120	353 - 374	0.120	764 - 809	0.120	992 - 1050	0.120		
27 - 30	0.133	74 - 80	0.133	114 - 120	0.133	252 - 266	0.133	374 - 394	0.133	809 - 852	0.133	1050 - 1105	0.133		
		80 - 86	0.147	120 - 127	0.147	266 - 280	0.147	394 - 413	0.147	852 - 894	0.147				
		86 - 91	0.160	127 - 133	0.160	280 - 293	0.160	413 - 431	0.160	894 - 933	0.160				
		91 - 97	0.174	133 - 140	0.174	293 - 306	0.174	431 - 449	0.174	933 - 972	0.174				
		97 - 104	0.187	140 - 146	0.187	306 - 318	0.187	449 - 466	0.187	972 - 1009	0.187				
		104 - 110	0.200	146 - 152	0.200	318 - 331	0.200	466 - 483	0.200	1009 - 1046	0.200				

Note:  $d\theta_T = \theta \gamma p \{ r_o - r_i + (f_i^2 + f_o^2 + z^2) \}$ ,  $r_i, r_o$  = inner, outer sector radii,  $\gamma = 6.67 \times 10^{-8}$ ,  $d\theta_T$  in milligals,  $z, f_i, f_o$  in feet, and  $z$  = average sector elevation.

Source: From Hammer (1939), but based on average density  $p = 2.67 \text{ g/cm}^3$ .

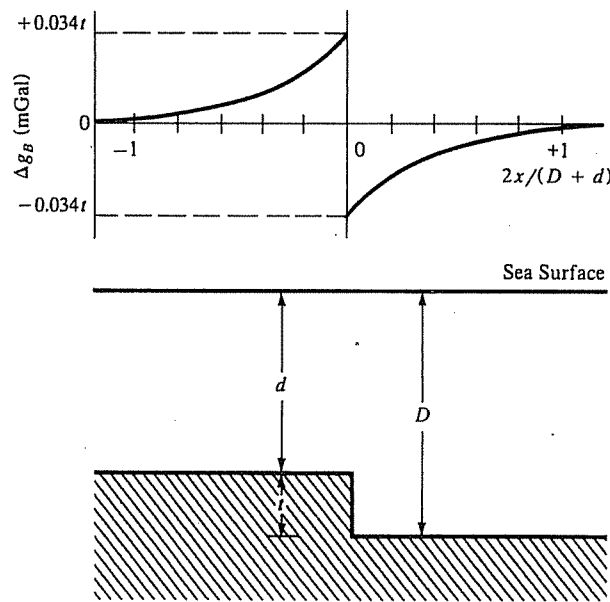


Figure 2.5. Marine terrain correction for vertical sea-floor step.  $\rho_w = 1.03$ ,  $\rho_{rock} = 2.67$ ,  $t$  = meters. (After Nettleton, 1971.)

usually it is included in the instrument drift correction (§2.5.2).

(g) *Isostatic correction.* The worldwide average of Bouguer anomalies on land near sea level is approximately zero. In regions of large elevation they are generally negative, while in oceanic regions mainly positive. These large-scale effects are due to density variations in the crust, indicating denser material beneath the ocean and less dense material in regions of elevated land.

In 1855, two hypotheses were put forward to account for the density variations. Airy proposed a crust of uniform density but variable thickness floating on a liquid substratum of higher density, whereas

Pratt suggested a crust where the density varies with topography, being lower in mountain regions and higher beneath the oceans. Both hypotheses appear to be true to some extent. An *isostatic correction* occasionally is necessary in large-scale surveys to compensate for crustal variations.

(h) *Bouguer and free-air anomalies.* When all of the preceding corrections have been applied to the observed gravity reading, we obtain the value of the *Bouguer anomaly*  $g_B$  for the station:

$$g_B = g_{\text{obs}} - g_t + (\Delta g_L + \Delta g_{FA} - \Delta g_B + \Delta g_T) \quad (2.28)$$

where  $g_{\text{obs}}$  is the station reading,  $g_t$  is the theoretical gravity,  $\Delta g_L$  is the latitude correction,  $\Delta g_{FA}$  is the free-air correction,  $\Delta g_B$  is the Bouguer correction, and  $\Delta g_T$  is the terrain correction. The correction terms in Equation (2.28) correspond to a station south of the reference latitude (in the northern hemisphere) and above the datum. Sometimes, rather than the value from Equation (2.20), some particular station value in the survey area is used for  $g_t$ . Note that the signs of  $\Delta g_{FA}$  and  $\Delta g_B$  change when the station is below the datum plane.

Another quantity that is sometimes used (especially with marine data) is the *free-air anomaly*, the value of  $g_B$  when  $\Delta g_B$  (and often  $\Delta g_T$ ) is omitted from Equation (2.28).

If the Earth had no lateral variations in density, after corrections for the preceding effects, gravity readings would be identical. The Bouguer and free-air anomalies result from lateral variations in density (see also Ervin, 1977).

### 2.3.3. Densities of Rocks and Minerals

The quantity to be determined in gravity exploration is local lateral variation in density. Generally density

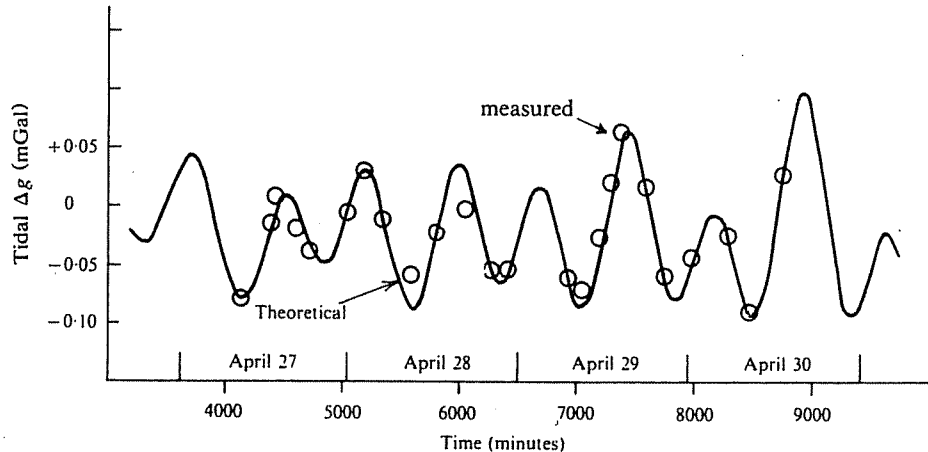


Figure 2.6. Earth-tide variations, Montreal, April 1969. Gravity readings have been corrected for instrument drift.

Table 2.2. Densities.

Rock type	Range (g/cm <sup>3</sup> )	Average (g/cm <sup>3</sup> )	Mineral	Range (g/cm <sup>3</sup> )	Average (g/cm <sup>3</sup> )
<b>Sediments (wet)</b>					
Overburden		1.92	<b>Metallic minerals</b>		
Soil	1.2–2.4	1.92	Oxides, carbonates	2.3–2.55	2.45
Clay	1.63–2.6	2.21	Bauxite	3.5–4.0	3.78
Gravel	1.7–2.4	2.0	Limonite	3.7–3.9	3.83
Sand	1.7–2.3	2.0	Siderite	4.18–4.3	4.25
Sandstone	1.61–2.76	2.35	Rutile	4.2–4.4	4.32
Shale	1.77–3.2	2.40	Manganite	4.3–4.6	4.36
Limestone	1.93–2.90	2.55	Chromite	4.3–5.0	4.67
Dolomite	2.28–2.90	2.70	Ilmenite	4.7–5.0	4.82
<b>Sedimentary rocks (av.)</b>			Pyrolusite	4.9–5.2	5.12
<b>Igneous rocks</b>			Magnetite	5.0–5.22	5.12
Rhyolite	2.35–2.70	2.52	Franklinite	4.9–5.3	5.18
Andesite	2.4–2.8	2.61	Hematite	5.7–6.15	5.92
Granite	2.50–2.81	2.64	Cuprite	6.8–7.1	6.92
Granodiorite	2.67–2.79	2.73	Cassiterite	7.1–7.5	7.32
Porphyry	2.60–2.89	2.74	Wolframite	3.5–4.0	3.75
Quartz diorite	2.62–2.96	2.79	Sphalerite	3.9–4.03	4.0
Diorite	2.72–2.99	2.85	Malachite	4.1–4.3	4.2
Lavas	2.80–3.00	2.90	Chalcopyrite	4.3–4.52	4.4
Diabase	2.50–3.20	2.91	Stannite	4.5–4.6	4.6
Basalt	2.70–3.30	2.99	Stibnite	4.5–4.8	4.65
Gabbro	2.70–3.50	3.03	Pyrrhotite	4.4–4.8	4.7
Peridotite	2.78–3.37	3.15	Molybdenite	4.7–4.9	4.85
Acid igneous	2.30–3.11	2.61	Marcasite	4.9–5.2	5.0
Basic igneous	2.09–3.17	2.79	Pyrite	4.9–5.4	5.1
<b>Metamorphic rocks</b>			Bornite	5.5–5.8	5.65
Quartzite	2.5–2.70	2.60	Chalcocite	5.8–6.3	6.1
Schists	2.39–2.9	2.64	Cobaltite	5.9–6.2	6.1
Graywacke	2.6–2.7	2.65	Arsenopyrite	6.5–6.7	6.57
Marble	2.6–2.9	2.75	Bismuthinite	7.4–7.6	7.5
Serpentine	2.4–3.10	2.78	Galena	8.0–8.2	8.1
Slate	2.7–2.9	2.79	Cinnabar	0.6–0.9	—
Gneiss	2.59–3.0	2.80	Ice	0.88–0.92	—
Amphibolite	2.90–3.04	2.96	Sea Water	1.01–1.05	—
Ectogite	3.2–3.54	3.37	Lignite	1.1–1.25	1.19
Metamorphic	2.4–3.1	2.74	Soft coal	1.2–1.5	1.32
			Anthracite	1.34–1.8	1.50
			Chalk	1.53–2.6	2.01
			Graphite	1.9–2.3	2.15
			Rock salt	2.1–2.6	2.22
			Gypsum	2.2–2.6	2.35
			Kaolinite	2.2–2.63	2.53
			Orthoclase	2.5–2.6	—
			Quartz	2.5–2.7	2.65
			Calcite	2.6–2.7	—
			Anhydrite	2.29–3.0	2.93
			Biotite	2.7–3.2	2.92
			Magnesite	2.9–3.12	3.03
			Fluorite	3.01–3.25	3.14
			Barite	4.3–4.7	4.47

is not measured *in situ*, although it can be measured by borehole logging tools (see §11.8.3). Density can also be estimated from seismic velocity (§4.2.8a). Often density measurements are made in the laboratory on small outcrop or drill-core samples. However, laboratory results rarely give the true bulk

density because the samples may be weathered, fragmented, dehydrated, or altered in the process of being obtained. Consequently, density is often not very well known in specific field situations.

Density data are given in Table 2.2. Sedimentary rocks are usually less dense than igneous and meta-

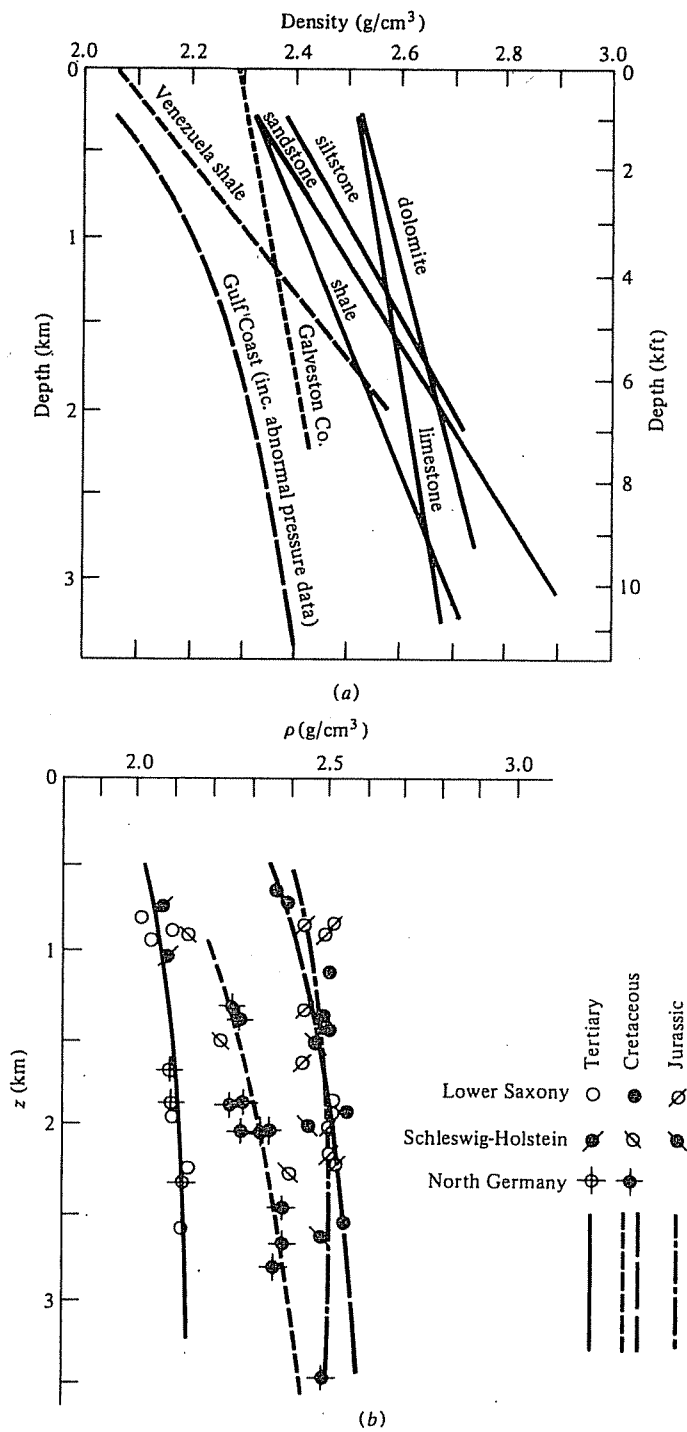


Figure 2.7. Density versus depth. (a) Western Hemisphere data: Venezuelan data from Hedberg (1936), Gulf Coast data from Dickenson (1953), Galveston County data from Bible (1964), and remaining data (Canadian) from Maxant (1980). (b) North Europe data from Hermes (1986).

morphic rocks. The wide range of density of sedimentary rocks is primarily due to variations in porosity. The nature of the pore fluids also affects the bulk density. Sedimentary rock density is also influenced by age, previous history, and depth of burial. Obviously a porous rock will be compacted when buried. In general, density increases with depth

(Fig. 2.7) and time. The density contrast between adjacent sedimentary formations in the field is seldom greater than  $0.25 \text{ g/cm}^3$  (except for the near-surface; §2.7.11).

Although igneous rocks generally are denser than sedimentary rocks, there is considerable overlap. Volcanics, particularly lavas, may have high porosi-

ties and, hence, low density. Generally, basic igneous rocks are heavier than acidic ones. Porosity, which affects the density of sediments so greatly, is of minor significance in most igneous and metamorphic rocks unless they are highly fractured.

Density usually increases with the degree of metamorphism because the process tends to fill pore spaces and recrystallize the rock in a denser form. Thus metamorphosed sediments, such as marble, slate, and quartzite, generally are denser than the original limestone, shale, and sandstone. The same is true for the metamorphic forms of igneous rocks, gneiss versus granite, amphibolite versus basalt, and so on.

With few exceptions, nonmetallic minerals have lower densities than the average for rocks ( $2.67 \text{ g/cm}^3$ ). Metallic minerals, on the other hand, mainly are heavier than this average, but since they rarely occur in pure form in large volumes, their effect normally is not great.

### 2.3.4. Density Estimates from Field Results

(a) *Density from underground measurements.* Sometimes it is feasible to make gravity measurements underground. If readings are taken at points directly below one another (for example, at the surface and in an underground opening), then the difference between these values is given by [see Eqs. (2.22) and (2.23)]

$$\Delta g = (0.3086 - 0.0838\rho) \Delta z + \varepsilon_T \text{ mGal}$$

$$\Delta g = (0.0941 - 0.0256\rho) \Delta z' + \varepsilon_T \text{ mGal}$$

where  $\Delta z$  is the elevation difference in meters,  $\Delta z'$  in feet,  $\rho$  is in grams per cubic centimeter, and  $\varepsilon_T$  is the difference in terrain corrections (due to air-filled mine tunnels) in milligals. (Note that the Bouguer correction has been doubled; see §2.3.2d.) Hence the average bulk density in the intervening rock is

$$\rho = 3.68 - 11.93(\Delta g - \varepsilon_T)/\Delta z \text{ g/cm}^3 \quad (2.29a)$$

or

$$\rho = 3.68 - 39.06(\Delta g - \varepsilon_T)/\Delta z' \text{ g/cm}^3 \quad (2.29b)$$

Because  $\varepsilon_T$  depends upon  $\rho$ , Equations (2.29) are usually solved by successive approximations.

Hussain, Walach, and Weber (1981) discuss underground surveys.

(b) *Density from borehole gravimeter measurements.* Borehole gravimeters (§11.9.1) are able to make gravity measurements to an accuracy of about  $5 \mu\text{Gal}$  (Schmoker, 1978; LaFehr, 1983). Terrain corrections are not necessary in borehole measurements. Differentiating Equations (2.29) keeping  $\Delta z$  and  $\Delta z'$  fixed gives

$$\Delta\rho = 0.0119(\Delta g/\Delta z) \text{ g/cm}^3 \quad (2.30a)$$

$$\Delta\rho = 0.0391(\Delta g/\Delta z') \text{ g/cm}^3 \quad (2.30b)$$

where  $\Delta g$  is in microgals. With meter accuracy of  $\pm 5 \mu\text{Gal}$ , the error in  $\Delta(\Delta g)$  can be as large as  $\pm 10 \mu\text{Gal}$ , and measuring density to  $\pm 0.01 \text{ g/cm}^3$  requires readings 12 m (40 ft) or more apart.

The volume contributing most to borehole gravity measurements is the portion closest to the borehole. Half of the effect is produced by rocks within a radius of  $0.7\Delta z$ , 80% from  $2.45\Delta z$  (the *radius of investigation*) and 90% from within  $5\Delta z$ . Borehole gravity measurements (LaFehr, 1983) permit determination of the density sufficiently far from the borehole so that invasion and alteration by the drilling process are unimportant, in contrast to the few inches of effective penetration achieved by other density logging tools. The main objective of borehole gravity measurements usually is to determine porosity, which is directly related to density.

(c) *Nettleton's method.* A reasonably satisfactory method of estimating near-surface density uses a gravity profile over topography that is not correlative with density variations (Nettleton, 1976). For example, a profile across an erosional valley that is not structure-controlled would probably be suitable, but a profile across a structure-controlled ridge might be suspect because density changes associated with the structure may correlate with elevation. Field readings are reduced to Bouguer gravity profiles assuming different values of  $\rho$  for the Bouguer and terrain corrections. The profile that reflects the topography the least is the one with the best estimate of the density. The method is illustrated in Figure 2.8; incorrect density assumptions result in profiles either following or inverting the topography. Obviously the density involved is that between the elevations of the highest and lowest stations.

(d) *Parasnis' method.* An analytical approach somewhat similar to Nettleton's graphical method has been developed by Parasnis (1962, p. 40). Rearranging Equation (2.28) and using Equation (2.25),

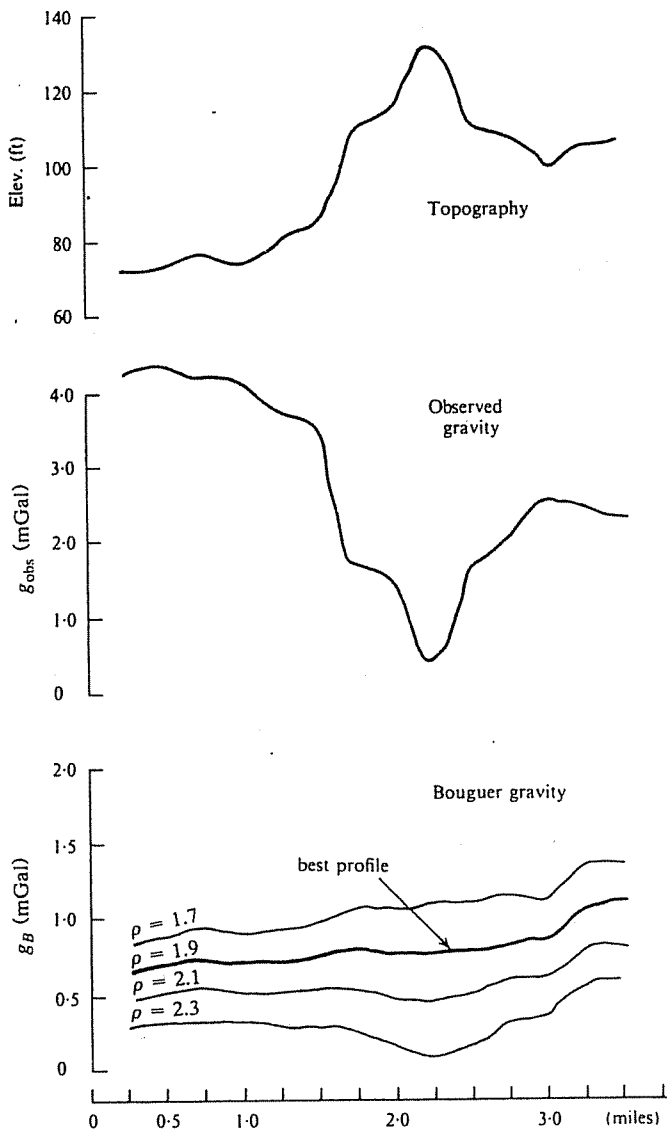


Figure 2.8. Method for estimating surface density.

we obtain

$$(g_{\text{obs}} - g_t + \Delta g_L + 0.3086z) - g_B = (0.0419z - \Delta g_T/\rho)\rho \quad (2.31a)$$

$$(g_{\text{obs}} - g_t + \Delta g_L + 0.0941z') - g_B = (0.0128z' - \Delta g_T/\rho)\rho \quad (2.31b)$$

where  $z$  is in meters and  $z'$  is in feet. We wish to determine the average bulk density for the data set by considering the Bouguer anomaly  $g_B$  to be a random error of mean value zero. If we plot

$$(g_{\text{obs}} - g_t + \Delta g_L + 0.3086z)$$

versus  $(0.0419z - \Delta g_T/\rho)$  (or the equivalent in terms

of  $z'$ ), the slope of the best-fit straight line through the origin will be  $\rho$ .

## 2.4. GRAVITY INSTRUMENTS

### 2.4.1. General

The absolute measurement of gravity is usually carried out at a fixed installation by the accurate timing of a swinging pendulum or of a falling weight.

Relative gravity measurements may be made in various ways. Three types of instruments have been used: the torsion balance, the pendulum and the gravimeter (or gravity meter). The latter is the sole instrument now used for prospecting, the others having only historical interest.

#### 2.4.2. Absolute Measurement of Gravity

Although the timing of a freely falling body was the first method of measuring  $g$ , the accuracy was poor because of the difficulty in measuring small time intervals. The method has been revived as a result of instrumentation improvements and elaborate free-fall installations are now located at several national laboratories. It is necessary to measure time to about  $10^{-8}$  s and distance to  $< \frac{1}{2} \mu\text{m}$  to obtain an accuracy of 1 mGal with a fall of 1 or 2 m.

Until recently, the standard method for measuring  $g$  employed a modified form of the *reversible Kater pendulum*. The value of  $g$  was obtained by timing a large number of oscillations.

#### 2.4.3. Relative Measurement of Gravity

(a) *Portable pendulum*. The pendulum has been used for both geodetic and prospecting purposes. Since  $g$  varies inversely as the square of the period  $T$ , we have

$$T^2 g = \text{constant}$$

Differentiating, we get

$$\begin{aligned}\Delta g &= -2g \Delta T/T \\ &= -2g(T_2 - T_1)/T_1\end{aligned}\quad (2.32)$$

Thus if we can measure the periods at two stations to about 1  $\mu\text{s}$ , the gravity difference is accurate to 1 mGal. This is not difficult with precise clocks such as quartz crystal, cesium, or rubidium.

The pendulum has been used extensively for geodetic work, both on land and at sea (in submarines). Portable pendulums used in oil exploration during the early 1930s had a sensitivity of about 0.25 mGal. Pendulum apparatus was complex and bulky. Two pendulums, swinging in opposite phase, were used to reduce sway of the mounting; they were enclosed in an evacuated, thermostatically controlled chamber to eliminate pressure and temperature effects. To get the required accuracy, readings took about  $\frac{1}{2}$  hr.

(b) *Torsion balance*. A fairly complete account of the salient features of the torsion balance can be found in Nettleton (1976). Figure 2.9 is a schematic of the torsion balance. Two equal masses  $m$  are separated both horizontally and vertically by rigid bars, the assembly being supported by a torsion fiber with an attached mirror to measure rotation by the deflection of a light beam. Two complete beam assemblies were used to reduce the effects of support sway. Readings were taken at three azimuth posi-

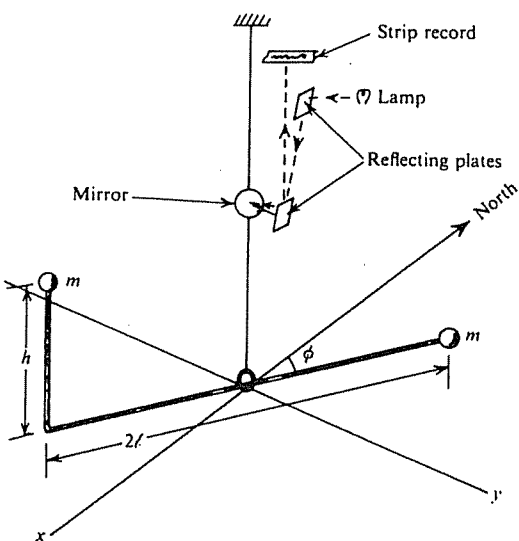


Figure 2.9. Torsion balance (schematic).

tions of the beam assemblies, normally  $120^\circ$  apart, to get sufficient data to calculate the required results. Elaborate precautions were required to minimize extraneous effects such as temperature and air convection. Each station had to be occupied for approximately one hour so that daily production was only 8 to 10 stations.

The deflection of the torsion balance beam is due to horizontal and vertical changes in the gravity field resulting from curvature of the equipotential surfaces. Torsion-balance measurements permitted calculation of  $U_{xy}$ ,  $U_{xz}$ ,  $U_{yz}$ , and  $|U_{yy} - U_{xx}|$ . The plotted values are usually the *horizontal gradient* [the vector  $(U_{xz}\mathbf{i} + U_{yz}\mathbf{j})$ ] and the *differential curvature* [a vector with magnitude given by Equation (2.19) and direction relative to the  $x$  axis of  $(1/2)\tan^{-1}(2U_{xy}/|U_{yy} - U_{xx}|)$ ]. Measurements were usually in Eötvös units (EU) equal to  $10^{-6}$  mGal/cm.

(c) *Stable-type gravimeters*. The first gravimeters dating from the early 1930s were of the stable type but these have now been superceded by more sensitive unstable meters. Nettleton (1976) describes a number of different gravimeters. All gravimeters are essentially extremely sensitive mechanical balances in which a mass is supported by a spring. Small changes in gravity move the weight against the restoring force of the spring.

The basic elements of a stable gravimeter are shown in Figure 2.10. Whereas the displacement of the spring is small, Hooke's law applies, that is, the change in force is proportional to the change in length; hence,

$$\Delta F = M \delta g = k \delta s \quad \text{or} \quad \delta g = k \delta s/M \quad (2.33)$$

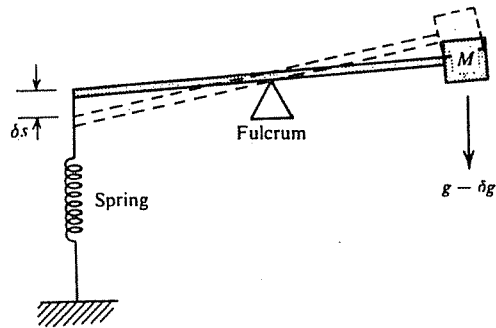


Figure 2.10. Basic principle of the stable gravimeter.

where  $k$  is the spring constant in dynes per centimeter. To measure  $g$  to 0.1 mGal, we must detect a fractional change in spring length of  $1/10^7$  (because  $Mg \approx ks$ ,  $\delta g/g \approx \delta s/s$ ), hence the need for considerable magnification. Mechanically we can make  $k/M$  small by using a large mass and a weak spring, but this method of enhancing sensitivity is limited. The period of oscillation of this system is

$$T = 2\pi(M/k)^{1/2}$$

Substituting for  $M$  in Equation (2.33), we get

$$\delta g = 4\pi^2 \delta s/T^2 \quad (2.34)$$

Thus for good sensitivity, the period is very large and measurement of  $\delta g$  requires considerable time. Stable gravimeters are extremely sensitive to other physical effects, such as changes in pressure, temperature, and small magnetic and seismic variations.

(d) *Unstable-type gravimeters*. Also known as *labilized* or *astatized* gravimeters, these instruments have an additional negative restoring force operating against the restoring spring force, that is, in the same sense as gravity. They essentially are in a state of unstable equilibrium and this gives them greater sensitivity than stable meters. Their linear range is less than for stable gravimeters so they are usually operated as null instruments.

The *Thyssen gravimeter*, although now obsolete, illustrates very clearly the astatic principle (Fig. 2.11). The addition of the mass  $m$  above the pivot raises the center of gravity and produces the instability condition. If  $g$  increases, the beam tilts to the right and the moment of  $m$  enhances the rotation; the converse is true for a decrease in gravity.

At present the Worden and LaCoste-Romberg meters are the only types used for exploration.

(e) *LaCoste-Romberg gravimeter*. The LaCoste-Romberg gravimeter was the first to employ a zero-length spring, now used by almost all gravimeters

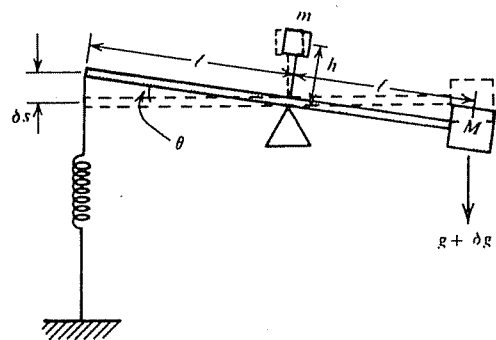


Figure 2.11. Basic principle of the unstable (Thyssen) gravimeter. (After Dobrin, 1960.)

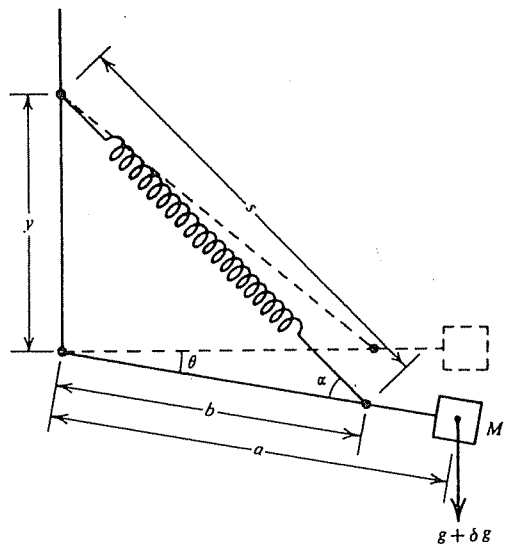


Figure 2.12. Lacoste-Romberg gravimeter.

(Askania, Frost, Magnolia, and North American). A *zero-length spring* is one in which the tension is proportional to the actual length of the spring, that is, if all external forces were removed the spring would collapse to zero length. The advantage of the zero-length spring is that if it supports the beam and mass  $M$  (see Fig. 2.12) in the horizontal position, it will support them in any position (note that  $\cos \theta$  in Eq. (2.35) cancels out, and  $g = K(1 - c/s)$ , which always has a solution since  $g$  is finite). Zero-length-springs are built with initial tension so that a threshold force is required before spring extension begins (as with a door spring).

To derive the expression for the sensitivity of the LaCoste-Romberg gravimeter, we write  $k(s - c)$  for the tension in the spring when its length is  $s$ ; thus,  $c$  is a small correction for the fact that the spring is not truly zero length. Taking moments about the pivot in Figure 2.12, we get

$$\begin{aligned} Mga \cos \theta &= k(s - c)b \sin \alpha \\ &= k(s - c)b(y \cos \theta)/s \quad (2.35) \end{aligned}$$

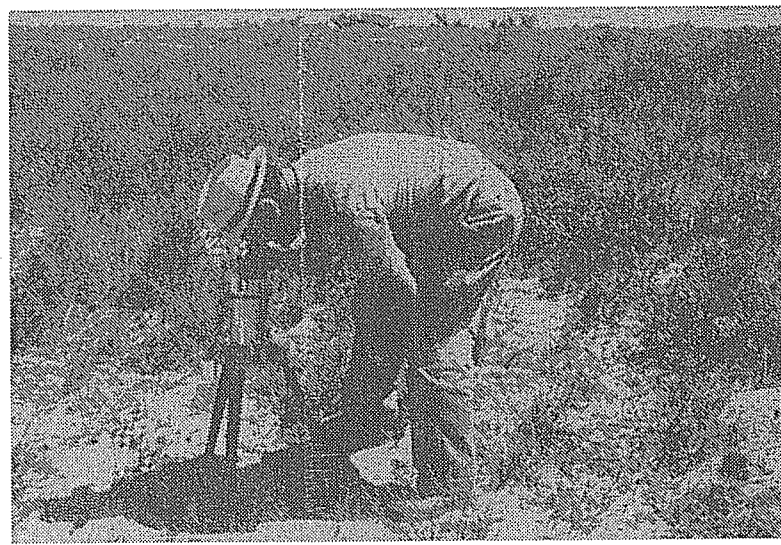


Figure 2.13. Reading a Worden gravimeter.

using the law of sines. Thus

$$g = (k/M)(b/a)(1 - c/s)y$$

When  $g$  increases by  $\delta g$ , the spring length increases by  $\delta s$  where

$$\delta g = (k/M)(b/a)(c/s)(y/s)\delta s \quad (2.36)$$

For a given change in gravity  $\delta g$ , we can make  $\delta s$  as large as we wish by decreasing one or more of the factors on the right-hand side; moreover, the closer the spring is to the zero-length spring, the smaller  $c$  is and the larger  $\delta s$  becomes.

In operation this is a null instrument, a second spring being used, which can be adjusted to restore the beam to the horizontal position. The sensitivity of gravimeters in use in surface exploration is generally 0.01 mGal. The instrument requires a constant-temperature environment, usually achieved by keeping it at a constant temperature that is higher than the surroundings.

(f) *Worden gravimeter.* The Worden gravimeter (Fig. 2.13) is especially portable and fast to operate. It uses small, very light weight parts of quartz (for example, the mass  $M$  weighs only 5 mg) with small inertia so that it is not necessary to clamp the movement between stations. Sensitivity to temperature and pressure changes is reduced by enclosing the system in a vacuum flask. The meter also employs an automatic temperature-compensating arrangement. The Worden meter is small (instrument dimensions are a few centimeters, the outer case is

about 25 cm high and 12 cm in diameter) and weighs about 2.5 kg. Its only power requirement is two penlight cells for illuminating the scale.

A simplified schematic is shown in Figure 2.14. The moving system is similar to the LaCoste-Romberg meter. The arm  $OP'$  and beam  $OM$  are rigidly connected and pivot about  $O$ , changing the length of the main spring  $P'C$ , which is fixed at  $C$ . We have the following relations:

$$\angle OCP' = \angle OP'C = \pi/2 - (\alpha + \theta/2)$$

$$RP \perp CP \quad P'P \perp OP$$

so

$$\angle RPP' = \pi/2 - \alpha$$

$$s = CP \quad \delta s = CP' - CP \approx b\theta \sin(\pi/2 - \alpha)$$

so

$$\theta \approx \delta s / (b \cos \alpha)$$

The correction factor  $c$  that appeared in the treatment of the LaCoste-Romberg meter is negligible for the Worden meter. Taking moments about the pivot for the case where  $\theta = 0$ , we get

$$Mga = ksb \cos \alpha$$

When  $g$  increases to  $(g + \delta g)$ ,  $P$  moves along the

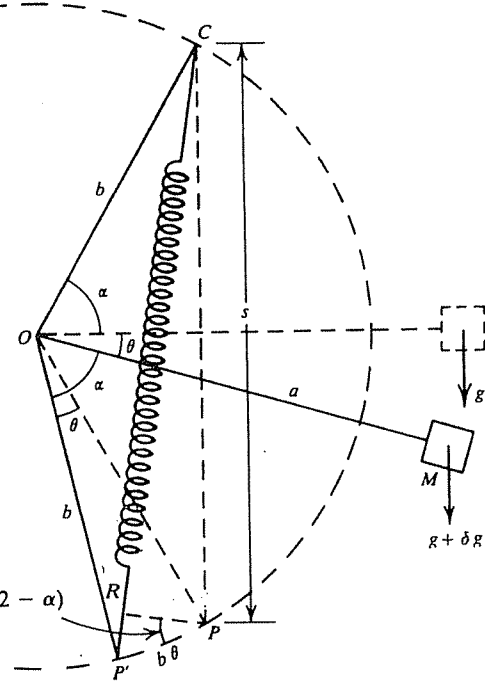


Figure 2.14. Basic principle of the Worden gravimeter.

circle to  $P'$  and

$$M(g + \delta g)a \cos \theta = kb(s + \delta s) \cos(\alpha + \theta/2)$$

When  $\theta \approx 0$ , to the first approximation this becomes

$$\begin{aligned} M(g + \delta g)a &= kb(s + \delta s)\{\cos \alpha - (\theta/2)\sin \alpha\} \\ &= kb(s + \delta s)\{\cos \alpha - (\delta s/2b)\tan \alpha\} \\ &= kb\{s \cos \alpha - \delta s(s/2b)\tan \alpha + \delta s \cos \alpha\} \end{aligned}$$

Subtracting the first moment equation to eliminate  $g$ , we get

$$Ma \delta g = kb\{\cos \alpha - (s/2b)\tan \alpha\} \delta s$$

Using the relation  $\sin \alpha = s/2b$ , we finally get

$$\delta g = (k/M)(b/a)(\cos 2\alpha/\cos \alpha) \delta s \quad (2.37)$$

As in the LaCoste-Romberg meter, the sensitivity can be increased by decreasing the factors  $(k/M)$  and  $(b/a)$ ; in addition the factor  $(\cos 2\alpha/\cos \alpha)$  approaches zero when  $\alpha$  approaches  $45^\circ$ , thus furnishing another method of obtaining high sensitivity. In practice the sensitivity is about 0.01 mGal.

Like the LaCoste-Romberg instrument, the Worden meter is read by measuring the force required to restore the beam to the horizontal position.

(g) Calibration of gravimeters. Both the Worden and LaCoste-Romberg meters are null instruments and changes in gravity are shown as arbitrary scale

divisions on a micrometer dial. There are several methods for converting these scale readings to gravity units.

Theoretically calibration can be carried out by tilting because a precise geometrical system is involved, but this is not the usual procedure. Generally, readings are taken at two or more stations where values of  $g$  are already known. If the value of  $\delta g$  between the stations is large enough to cover a reasonable fraction of the instrument range, a linear response is usually assumed between them. However, one should occupy several additional stations if possible.

## 2.5. FIELD OPERATIONS

### 2.5.1. Land Surveys

Gravity exploration is carried out both on land and at sea. Although some attempts have been made to develop an airborne instrument, this mode of operation is not yet practical (Paterson and Reeves, 1985).

The distinction between reconnaissance and detailed field work is based on the objective, that is, whether the purpose is to find features of interest or to map them. Station spacings in field work with the gravimeter vary from 20 km to as little as 5 m. The station interval is usually selected on the basis of assumed depth and size of the anomalies sought. For oil exploration, one station per 2 to 4 km<sup>2</sup> is desirable because structures associated with oil accumulation are usually larger than this and hence their

anomalies would not be missed with such spacing. While a more-or-less uniform grid of stations is desirable, stations are often run on loops that are operationally easier. Stations 0.5 to 1.0 km apart on loops roughly  $6 \times 6$  km in size might be typical for a petroleum survey.

In mineral exploration, gravity is normally employed as a secondary detail method for confirmation and further analysis of anomalies already outlined by magnetic and/or electrical techniques. The spacing is determined mainly by knowledge gained from the earlier surveys. Measurements are usually made at the same locations as the magnetic or electrical stations, commonly 15 to 30 m apart.

*Microgravity* engineering and archaeological surveys (for example, searching for cavities or bedrock) sometimes involve station spacing as close as 1 m (Arzi, 1975).

Field measurements with modern gravimeters are straightforward. The gravimeter must be leveled precisely for each reading. It may be difficult to get a stable null in swampy ground and when the wind is strong, but extra care and time generally give an acceptable measurement. Similar problems arise in marine gravity work using instruments that rest on the sea floor. For reasonable speed of operation, a vehicle normally is used for getting from station to station.

Precision is required in surveying gravity stations. Achieving the required precision (10 cm in elevation and about 30 m in latitude for 0.03 mGal accuracy) often involves the major cost of field work. Gravity measurements typically proceed much faster than the surveying, and three or four survey teams may be required to keep ahead of one meter operator.

*Inertial navigation* sometimes cuts the cost of determining location and elevation, especially where helicopter transport is used in areas of difficult access (LaFehr, 1980). An inertial navigation system (§B.7) senses acceleration by means of three orthogonal accelerometers mounted on a gyroscopically stabilized platform; changes in horizontal and vertical position are determined by integrating twice over time. Very small errors tend to accumulate rapidly to produce large errors, but these can be reduced to acceptable amounts if the helicopter stops every 3 to 5 min during which time the drift rate can be determined. This time interval is compatible with the travel time from station to station. Lynch and King (1983) claim 0.8 m elevation accuracy and 15 m horizontal accuracy in a survey in the mountainous overthrust belt of the Rocky Mountains, to yield Bouguer values with 0.3 mGal accuracy. In a high-precision survey of a limited area in northern Canada checked by leveling, elevations were determined to

0.9 m and horizontal positioning to 0.43 m, so inertial navigation can achieve remarkable accuracy. With a helicopter survey, stations can be located on a more uniform grid than with land surveys (which are usually run around the perimeter on traverses), so that interpolation errors are considerably reduced.

### 2.5.2. Drift Correction

Gravimeters change their null reading value gradually with time. This *drift* results mainly from creep in the springs and is usually unidirectional. Modern instruments, however, have very little drift. Gravity readings also change with time because of tidal effects (§2.3.2f).

The net result of drift and tidal effects is that repeated readings at one station give different values. *Drift correction* is accomplished by reoccupying some stations. The maximum time between repeat readings depends on the accuracy desired, but is usually 3 or 4 hr. A drift curve is shown in Figure 2.15. Its oscillatory shape is determined by tidal effects. It is not necessary to use the same station for checking drift because any station can be reoccupied. Intermediate gravity stations occupied only once can then be corrected for the drift that occurred.

If the meter movement is not clamped between readings or is subjected to sudden motion or jarring (as during transport), somewhat erratic changes (called *tears* or *tares*) may be produced. If the instrument is bumped, it is wise to reread a known station immediately. Since there is no way of allowing for erratic changes, we can only correct those points occupied while the drift curve is smooth.

### 2.5.3. Marine Surveys

(a) *Locating marine stations.* Considerable gravity work has been done on the surface of water-covered areas and also on the sea floor. Locating the station is usually done by using a radionavigation system such as Shoran, Raydist, or RPS (see §B.6). The accuracy of offshore location is usually lower than on land but elevation determination is not a problem if appropriate allowance is made for tidal variations.

(b) *Remote control systems.* Standard gravimeters have been adapted for operation on the sea floor to depths of 200 m. This method of measurement is suitable for most inland waters and coastal areas. The meter is enclosed in a pressure housing that is supported on a squat tripod with disk feet. About

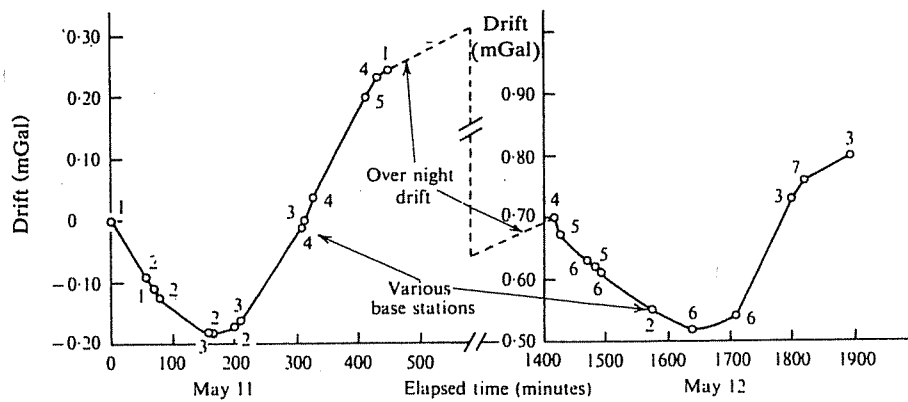


Figure 2.15. Gravimeter drift during a field survey.

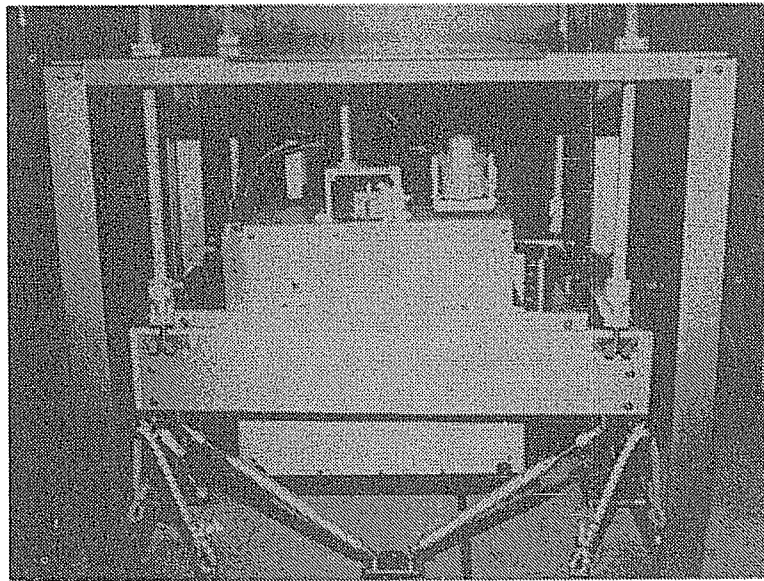


Figure 2.16. Photograph of a shipboard gravimeter.

half the total weight of the assembly is in the tripod in order to provide maximum stability when it is resting on the bottom; the overall weight of one model is 300 kg. The assembly is connected to a ship by a cable from which it is lowered into position on the bottom. Leveling is achieved by small motors that raise or lower the disk feet.

Although the high sensitivity of this equipment is an advantage, operation in deep water is slow because the assembly must be raised to the surface between stations. A problem in reoccupying stations is that the sea floor location may be different from that previously occupied, even when the surface location is identical. This method is now little used.

(c) *Shipboard operations and the Eötvös correction.* Shipboard gravimeters (Fig. 2.16) are used for most gravity measurements at sea. Shipboard gravimeters are mounted on an elaborate gyro-stabilized platform (Valiant and LaCoste, 1976) located in the part of a ship where there is minimum movement due to roll and pitch.

If a gravimeter has a velocity during a measurement, the centrifugal force acting on the meter is different from that when it is at rest. An eastward component of velocity adds to the velocity owing to the rotation of the Earth and hence increases the centrifugal force and decreases the gravity reading. A westward component of velocity has the opposite

effect. A northward component creates a new component of centrifugal force, which is added vectorially to the first. The correction for the velocity of the meter,  $\Delta g_V$ , called the *Eötvös correction*, is given by

$$\Delta g_V = 4.040V \cos \phi \sin \alpha + 0.001211V^2 \text{ mGal} \quad (2.38a)$$

$$\Delta g_V = 7.503V' \cos \phi \sin \alpha + 0.004154V'^2 \text{ mGal} \quad (2.38b)$$

where  $V$  is in kilometers per hour,  $V'$  in knots,  $\phi$  is the latitude, and  $\alpha$  is the course direction with respect to true north. The accuracy of shipboard gravity depends mainly on the accuracy of the Eötvös correction.

The error in the Eötvös correction due to errors in  $V$  and  $\alpha$  is

$$\begin{aligned} d(\Delta g_V) &= (0.0705V \cos \phi \cos \alpha) d\alpha \\ &\quad + (4.040 \cos \phi \sin \alpha + 0.002422V) dV \end{aligned} \quad (2.39)$$

with  $V$  and  $dV$  in kilometers per hour and  $d\alpha$  in degrees. Thus the sensitivity to velocity error is greatest for an east-west course and the sensitivity to course-direction error is greatest for a north-south course. Assuming that the velocity at the moment of gravity reading involves an uncertainty of 0.2 km/hr and instantaneous heading error of  $1^\circ$ ,  $\phi = 40^\circ$ , and  $V = 10$  km/hr, then  $d(\Delta g_V) = 0.62$  mGal for an east-west course and 0.54 mGal for a north-south course.

#### 2.5.4. Airborne Gravity

The main difficulty with airborne gravity surveys arises from very large and rapid changes in  $g_{\text{obs}}$  caused by changes in the aircraft altitude, linear acceleration, roll, and heading. These effects can be corrected for in shipborne gravity work because changes are slow and the velocity is low.

Hammer (1983) tells of using a helicopter flying (in the middle of the night to avoid air turbulence) at a speed of 50 to 100 km/hr at elevations of 300 to 4,000 m using an autopilot directed by a navigation-system computer (a human pilot is not sufficiently precise). His data, smoothed over a 2 min window (2 to 4 km), suggest that airborne gravity would be

useful for regional studies and reconnaissance of large anomalies. Brozena (1984) achieved an accuracy of 5 mGal averaged over 20 km.

## 2.6. GRAVITY DATA PROCESSING

### 2.6.1. Noise, Regionals, and Residuals

Because a Bouguer map shows horizontal differences in the acceleration of gravity, only horizontal changes in density produce anomalies. Purely vertical changes in density produce the same effect everywhere and so no anomalies result.

The gravity field is a superposition of anomalies resulting from density changes (anomalous masses) at various depths. Some anomalous masses lie at depths in the zone of interest, some result from deeper masses, and some from shallower ones. As the source of an anomaly deepens, the anomaly becomes more spread out and its amplitude decreases. The smoothness (or apparent wavelength) of anomalies is generally roughly proportional to the depth of the lateral density changes.

The depth range we wish to emphasize depends on the objectives of the interpretation. Shallow anomalies are of interest in mineral exploration but are usually regarded as undesirable noise in petroleum exploration. As in any geophysical technique, the most useful factor in interpretation is knowledge of the local geology.

Whereas it is possible for a distributed anomalous mass to give an anomaly that appears to originate from a more concentrated deeper mass, a concentrated mass cannot appear to originate deeper. The horizontal extent and smoothness of an anomaly is therefore usually a measure of the depth of the anomalous mass, and this property can be used to partially separate the effects of anomalous masses that lie within a depth zone of interest from the effects of both shallower and deeper masses.

The effects of shallow masses (*near-surface noise*) are usually of short wavelength. They can be removed largely by filtering out (smoothing) short-wavelength anomalies. The effects of deep masses are called the *regional*. The gravity field after near-surface noise and the regional have been removed is called the *residual*; it presumably represents effects of the intermediate zone of interest.

The major problem in gravity interpretation is separating anomalies of interest from the overlapping effects of other features; usually the main obscuring effects result from deeper features. *Residualizing* attempts to remove the regional so as to emphasize the residual. However, the separation usu-

ally is not complete; both regional and residual are distorted by the effects of each other.

Residualizing can also be thought of as predicting the values expected from deep features and then subtracting them from observed values, so as to leave the shallower effects. The expected value of the regional is generally determined by averaging values in the area surrounding the station. Several methods of removing the unwanted regional are described in the next section. Gupta and Ramani (1982) discuss the application of different residualizing methods.

Gravity station locations should be shown on the final map to aid in distinguishing residuals that are well controlled from those possibly resulting from interpolation.

The result obtained by smoothing profiles or contours is inevitably biased by the interpreter, but this is not necessarily bad. If the interpreter is experienced and uses additional geologic knowledge to guide him, it may be a decided advantage. It should be noted that nonsmoothing methods of residualizing also involve subjective elements, such as the choice of order for surface fitting, of grid dimensions in grid residualizing, and so on.

## 2.6.2. Graphical Residualizing

Graphical residualizing is done by smoothing either profiles or maps. A simple example of removing the regional by smoothing is illustrated in Figure 2.17. The profile in Figure 2.17a shows disturbances of different sizes; the smooth, nearly linear slope is the regional. In Figure 2.17b, the regional contours are regular and the residual obtained by subtracting the smoothed contours from the map values should be reliable.

The emphasis in drawing a smooth regional should be on "smooth" and most of the errors or failures in residualizing are caused by the regional not being sufficiently smooth. "Smooth" implies both smooth in shape and systematic in contour interval. Often profiles are plotted for several parallel lines, generally in the dip direction. Smooth regionals are then drawn on these parallel lines, making certain that they are consistent on all profiles. Often cross profiles are drawn linking the parallel lines into a grid to ensure that the regional is consistent over the grid. This approach is especially suitable when the regional trend is mainly unidirectional. If the survey has been carried out with close, uniform spacing of stations and lines, the station values themselves can be used instead of contour values to plot the profiles, thereby reducing errors because of contour interpolation.

Once the regional has been contoured, the residuals are obtained by subtracting the regional from the Bouguer map, either graphically or numerically. Graphical residualizing is sometimes done by drawing contours of constant difference through the points where regional and observed contours intersect.

When the regional is so irregular that the directional trend is not immediately apparent or when there are several superimposed regional systems, residualizing may be done iteratively, that is, one first determines and removes the most obvious regional and then finds a second-order regional from the first-order residual, and so on.

## 2.6.3. Surface-Fitting Residualizing Methods

The regional is sometimes represented by a low-order analytic surface. The parameters of the analytic surface are usually determined by a least-squares fit (Agocs, 1951) or some similar operation. How closely the surface fits the data depends on the order of the surface and the magnitude of the area being fitted. Nettleton (1976) illustrates orders of fit for a one-dimensional case (Fig. 2.18). The regional surface is often that given by a polynomial or the low-order components of a 2D-Fourier surface [Eq. (A.52a)]. The selection of order is usually made by examination of trial fits of several different orders.

Surface fitting is sometimes done to isolate and emphasize trends. Results from Coons, Woolard, and Hershey (1967) are shown in Figure 2.19. The trend becomes more evident as the order increases up to some point, about tenth order for the data of Figure 2.19. The residual for low order still contains appreciable regional trend and thus low orders are not very effective in separating the regional from the residual. Likewise, high-order surfaces are not effective because much of the sought-after anomaly is mixed with the regional in the surface fit.

## 2.6.4. Empirical Gridding Methods

Gridding provides a simple way of predicting the regional by regarding it as the average value of gravity in the vicinity of the station (Griffin, 1949). Usually the values averaged are those on the circumference of a circle centered at the station:

$$\overline{g(r)} = (1/2\pi) \int_0^{2\pi} g(r, \theta) d\theta \quad (2.40)$$

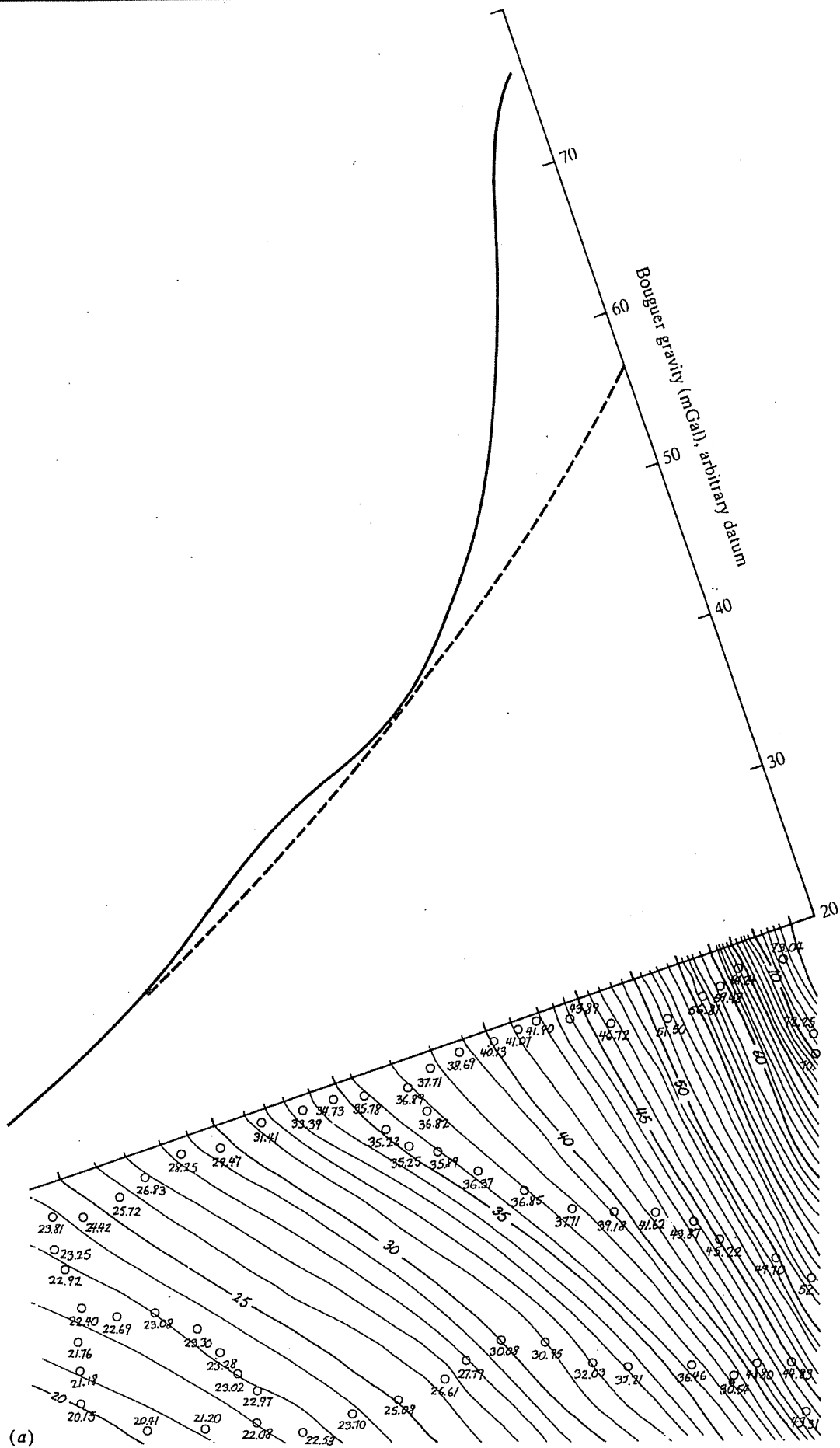


Figure 2.17. Graphical residualizing (After Sheriff, 1978). (a) Removing the regional on a profile across a local uplift and a fault.

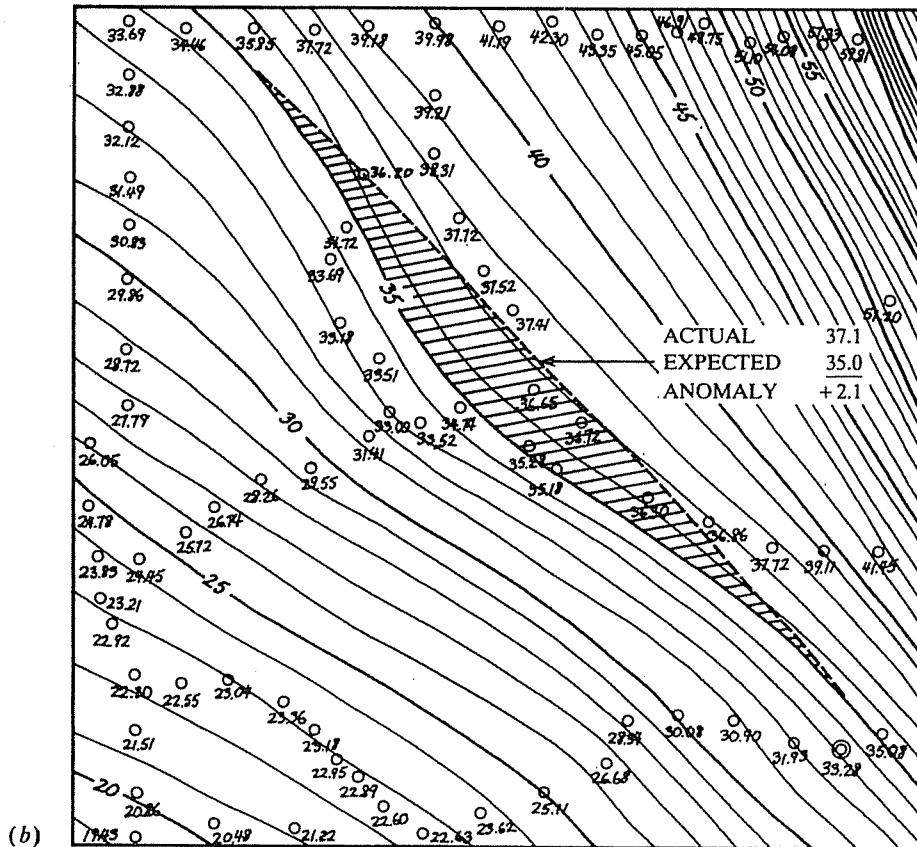


Figure 2.17. (Continued) (b) Removing the regional by contour smoothing.

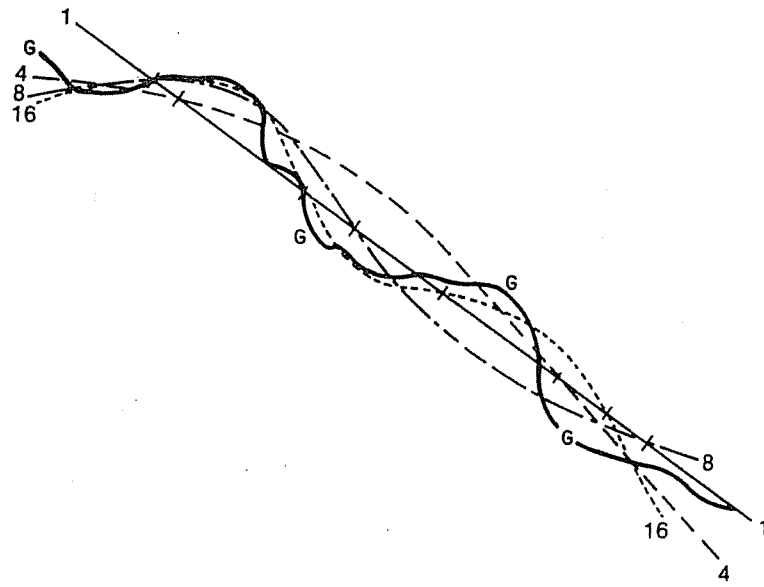


Figure 2.18. Illustrating least-squares surface-fitting. Curve G represents a gravity profile and curves 1, 4, 8, 16 represent fits of the respective orders. The surface fit, and hence the residual, depends on the dimensions that are fitted (from Nettleton, 1976).

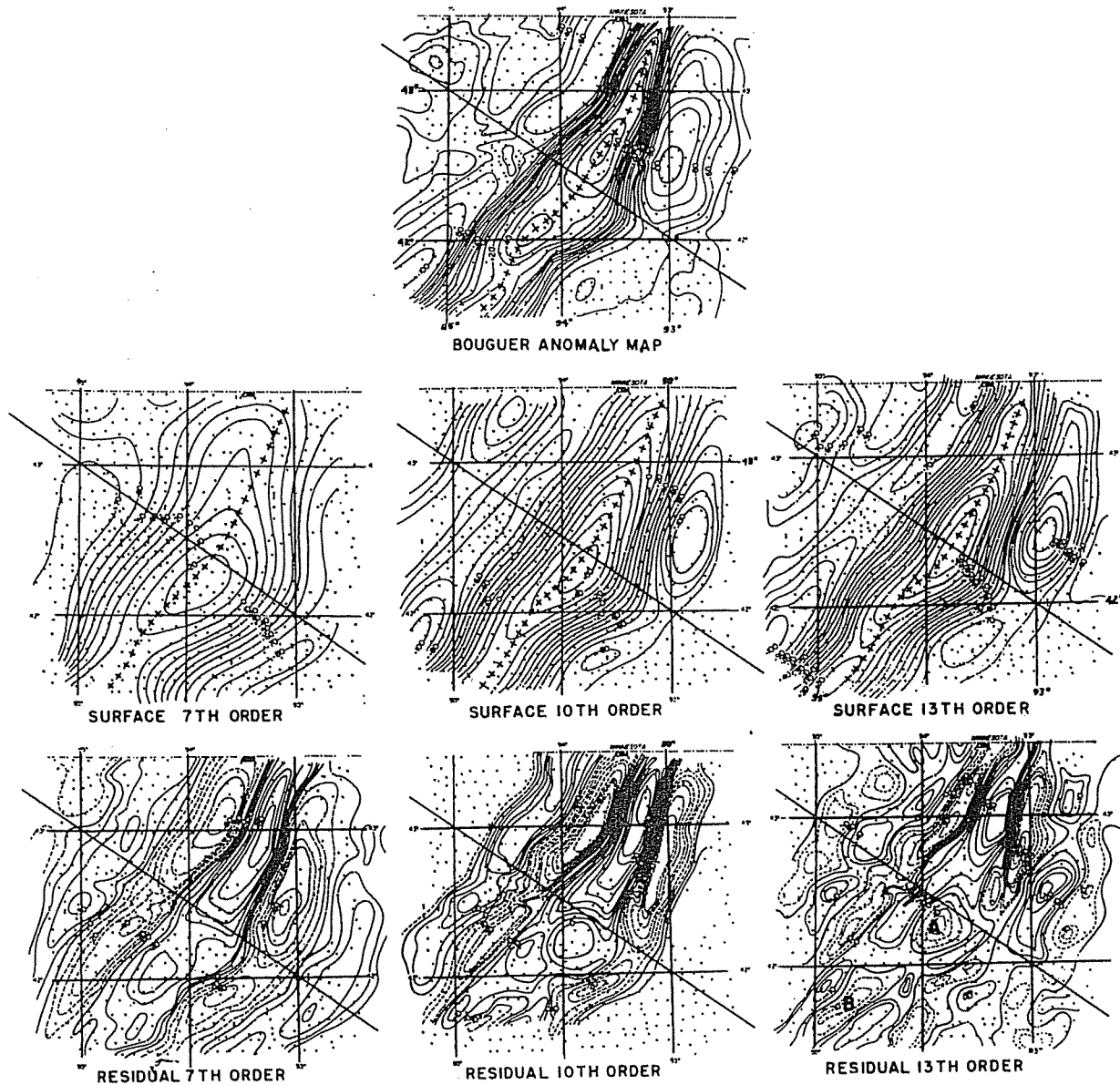


Figure 2.19. Fits of surfaces of different order and the respective residuals. (After Coons, Woolard, and Hershey, 1967.)

In actual practice the integral is generally replaced by a sum of discrete values (as in Fig. 2.20a):

$$\bar{g}(r) = \{g(r, 0) + g(r, \theta_1) + \dots + g(r, \theta_{n-1})\} / n \quad (2.41)$$

where  $\theta_m = m(2\pi/n)$ . The residual is then

$$g_r = g_B - \bar{g}(r) \quad (2.42)$$

where  $g_B$  is the Bouguer anomaly value. Usually the values of  $g(r, \theta_m)$  are obtained by interpolation from the gravity map contours. The result depends somewhat on the number of points selected but even more on the radius of the circle. If the radius is so small

that part of the anomaly is included on the circle, then the anomaly magnitude will be too small; if the radius is too large, the average may be biased by other anomalies. The radius is usually of the same order of magnitude as the depth of the anomaly to be emphasized, but both shallower and deeper anomalies will still contribute to the results. The grid spacing for points to be calculated is generally about half the radius used for averaging.

Sometimes averages over several circles of different radii  $r_i$  are used; successive circles are assigned different weights,  $w_i$ :

$$g_r = (c/s^2) \{ g_0 + w_1 \bar{g}(r_1) + w_2 \bar{g}(r_2) + \dots \} \quad (2.43)$$

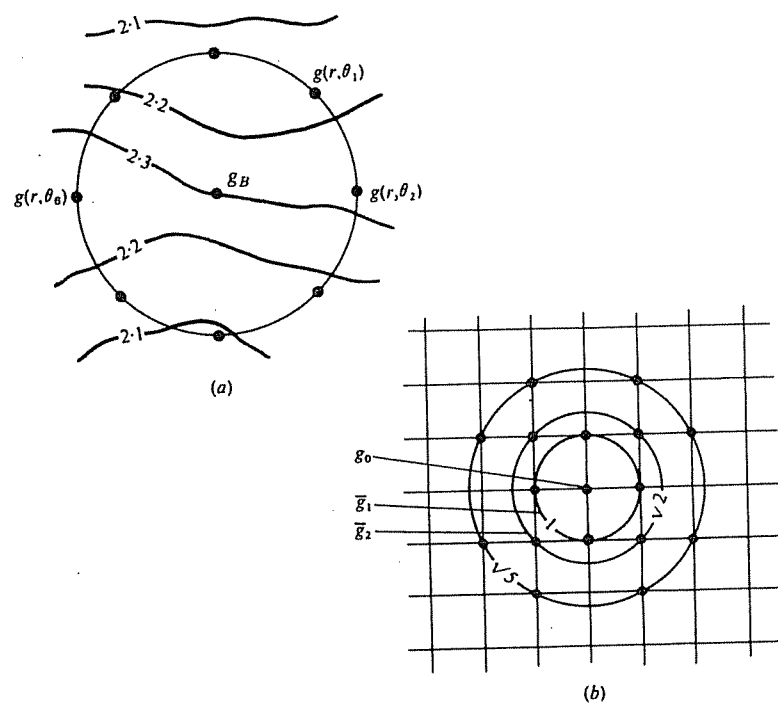


Figure 2.20. Analytical separation of the residual and the regional. (a) Griffin method.  
(b) Second-derivative method.

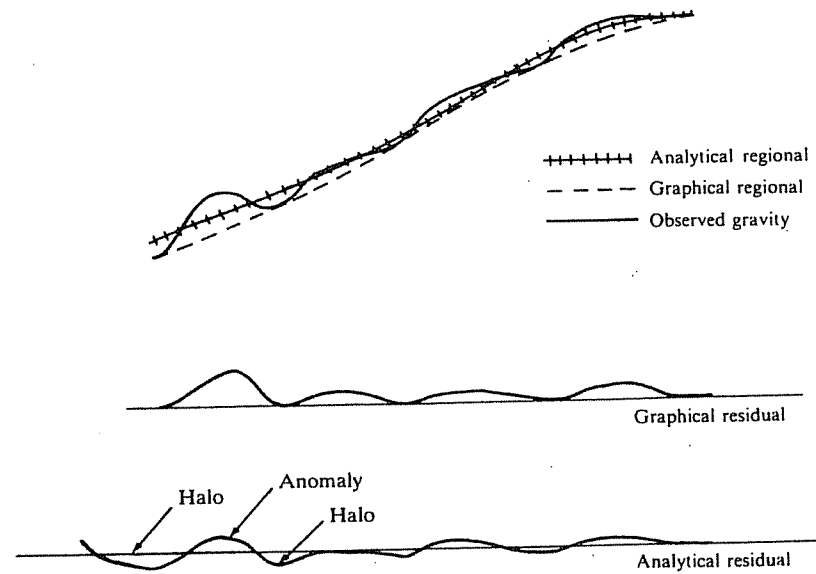


Figure 2.21. Comparison of graphical and analytical methods of removing regional gravity.

where  $c$  is a constant,  $s$  is a scale factor, and  $\sum w_i = -1$ . Usually the values on the various circles are read at grid points as in Figure 2.20b. Equation (2.43) is simply the expression for a 2-D convolution, and residualizing can be thought of as a convolution or filtering operation.

In graphical methods the interpreter usually draws the regional so that all residuals are either positive or

negative according to his concept of the density contrast expected to cause the anomaly. However, in nongraphical methods, the average value of the residual is usually set at zero so that both positive and negative residuals result. This is illustrated in Figure 2.21. A consequence of this is that each anomaly is surrounded by a "halo" of opposite sign, which does not indicate a separate anomaly.

### 2.6.5. Second Vertical Derivative Methods

The second vertical derivative enhances near-surface effects at the expense of deeper anomalies. Second derivatives are a measure of curvature, and large curvatures are associated with shallow anomalies.

The second vertical derivative can be obtained from the horizontal derivatives because the gravity field satisfies Laplace's equation

$$\nabla^2 g = \partial^2 g / \partial x^2 + \partial^2 g / \partial y^2 + \partial^2 g / \partial z^2 = 0$$

$$\partial^2 g / \partial z^2 = -(\partial^2 g / \partial x^2 + \partial^2 g / \partial y^2) \quad (2.44)$$

For the one-dimensional case, the first derivative can be estimated by dividing the difference between readings at two nearby locations,  $x_1$  and  $x_2$ , separated by the distance  $\Delta x$ :

$$dg(x_{1.5})/dx \approx \{g(x_2) - g(x_1)\}/\Delta x$$

The second derivative is obtained from the difference between nearby first derivatives:

$$\begin{aligned} d^2g(x_2)/dx^2 &\approx \{dg(x_{2.5})/dx - dg(x_{1.5})/dx\}/dx \\ &\approx [\{g(x_3) - g(x_2)\}/\Delta x \\ &\quad - \{g(x_2) - g(x_1)\}/\Delta x]/\Delta x \\ &\approx \{g(x_3) - 2g(x_2) \\ &\quad + g(x_1)\}/(\Delta x)^2 \end{aligned} \quad (2.45)$$

Equation (2.45) has the same form as Equation (2.43) (a weighted sum of the values at nearby points), and Equation (2.43) yields an estimate of the second vertical derivative for appropriate values of  $w_i$ .

A number of mathematical treatments have been developed (Henderson and Zietz, 1949; Elkins, 1951; Dean, 1958) to extract the vertical second derivative from the average values at various distances from the station. Generally values over concentric circles are weighted to produce an expression of the form [compare with Eq. (2.43)]

$$\partial^2 g / \partial z^2 = (c/s^2)(w_0 g_0 + w_1 \bar{g}_1 + w_2 \bar{g}_2 + \dots) \quad (2.46a)$$

where  $g_0$  is the gravity at the station where the second derivative is being determined,  $\bar{g}_1, \bar{g}_2, \dots$  are averages over surrounding circles of various radii,  $w_0, w_1, \dots$  are weighting coefficients such that  $\sum w_i = 0$ ,  $c$  is a numerical factor, and  $s$  is the grid spacing. For example, if the survey is on a square grid and the successive radii are  $s$ ,  $s\sqrt{2}$ , and  $s\sqrt{5}$  (as in Fig. 2.20b), one form of equation (2.46a) is

$$\partial^2 g / \partial z^2 = 2(3g_0 - 4\bar{g}_1 + \bar{g}_2)/s^2 \quad (2.46b)$$

(Henderson and Zietz, 1949). Gupta and Ramani (1982) show an application to mineral exploration.

### 2.6.6. Wavelength Filtering

The foregoing methods of separating residuals from the regional are based on the degree of smoothness (or wavelength = 1/wavenumber; see §4.2.2d) of anomalies. Filtering can also be done by transforming map data to a wavenumber-wavenumber domain using a two-dimensional Fourier transform [Eqs. (A.57)], removing certain wavenumber components (that is, filtering), and then doing an inverse transformation to reconstitute the map, but with certain wavelengths removed. What are removed are usually the small wavenumbers (large wavelengths) of the regional, so that the wavenumber components involved in the inverse transform are the large ones which correspond to the short wavelengths of the residual.

Wavenumber filtering encounters the same problem as other residualizing schemes. The wavenumber spectra of most features are broadband, so spectra of features at different depths overlap and consequently the features cannot be separated completely by filtering.

### 2.6.7. Field Continuation

The fact that gravity fields obey Laplace's equation permits us to determine the field over an arbitrary surface if the field is known completely over another surface and no masses are located between the two surfaces. This process is called *continuation*.

Following the method of Grant and West (1965, pp. 216–21), we let the plane  $z = 0$  separate free space ( $z < 0$ ) from the region containing masses ( $z > 0$ ) (Fig. 2.22a);  $P$  is a point in free space,  $Q$  locates a point mass, and  $R$  is the distance  $PQ$ . If  $U_P$

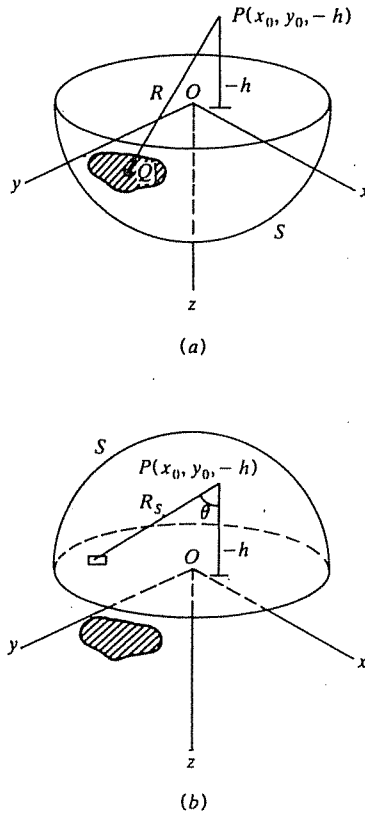


Figure 2.22. The continuation theorem. (After Grant and West, 1965.) (a) Hemisphere  $S$  on positive side of  $xy$  plane. (b) Hemisphere on negative side of  $xy$  plane.

and  $U_Q$  are the potentials at  $P$  and  $Q$ , Equations (2.6a) and (2.13b) give

$$U_P = \gamma \int_V (\rho/R) dv$$

$$\nabla^2 U_Q = -4\pi \gamma \rho$$

Eliminating  $\rho$ , we have

$$U_P = -(1/4\pi) \int_V (1/R) \nabla^2 U_Q dv$$

We now apply Green's theorem [Eq. (A.28)] to the hemisphere in Figure 2.22a with  $W = 1/R$ ,  $U = U_Q$  inside  $S$ , and  $U = U_S$  on the surface. Since  $\nabla^2(1/R) = 0$ , we get

$$-\int_V (1/R) \nabla^2 U_Q dv = 4\pi U_P = \int_S \{ U_S \nabla(1/R_S)$$

$$-(1/R_S) \nabla U_S \} \cdot ds$$

$$= \int_S \{ U_S \partial/\partial n (1/R_S)$$

$$-(1/R_S) \partial U_S / \partial n \} ds$$

The derivatives within the braces are the components of the gradients normal to the surface  $ds$ . Setting the radius of the hemisphere equal to infinity causes the contribution of the curved surface to vanish because of the factor  $1/R_S$ , and the integral reduces to

$$4\pi U_P = \int_{x,y} \{ U_S (\partial/\partial n) (1/R_S)$$

$$-(1/R_S) \partial U_S / \partial n \} dx dy \quad (2.47a)$$

The integration is taken over that portion of the  $xy$  plane where the anomalous field is significantly larger than zero.

We now follow the same procedure using the hemisphere in Figure 2.22b. Because  $\nabla^2 U_Q = 0$  within the hemisphere [Eq. (2.11a)], we get

$$0 = \int_{x,y} \{ U_S (\partial/\partial n) (1/R_S)$$

$$-(1/R_S) \partial U_S / \partial n \} dx dy \quad (2.47b)$$

The right-hand sides of Equations (2.47a) and (2.47b) appear to be the same, but, in fact, they are different because  $n$ , the outward unit normal to the surface  $ds$ , is upward ( $-z$  direction) in Equation (2.47a) and downward ( $+z$  direction) in Equation (2.47b). Thus,  $\partial U_S / \partial n = -g$  in Equation (2.47a) and  $+g$  in Equation (2.47b). Also,  $R_S^2 = (x - x_0)^2 + (y - y_0)^2 + (z + h)^2$ , so, on the  $xy$  plane,

$$(\partial/\partial n)(1/R_S) = \lim_{z \rightarrow 0} (\partial/\partial z)(1/R_S)$$

$$= \lim_{z \rightarrow 0} \{ -(z + h)/R_S^3 \}$$

$$= -h/R_S^3$$

which is independent of the direction of  $n$ . Thus, subtracting Equation (2.47b) from (2.47a), we obtain

$$U_P = (1/2\pi) \int_{x,y} (g/R_S) dx dy$$

where  $R_S^2 = (x - x_0)^2 + (y - y_0)^2 + h^2$ . To get  $\partial U_P / \partial z$  at  $P$ , we replace  $h^2$  in  $R_S^2$  with  $z^2$ , differentiate, and then replace  $z$  with  $(-h)$  (note that  $g$  on the  $xy$  plane is not a function of  $z$ ). The result is

$$\partial U_P / \partial z = g_P = (1/2\pi) h \int_{x,y} (g/R_S^3) dx dy \quad (2.48)$$

Since  $(h/R_S) = \cos \theta$  in Figure 2.22b,  $(g/2\pi)$  can be regarded as a surface density of mass replacing the mass below the  $xy$  plane [compare with Eq. (2.14)]. Equation (2.48) is the *upward continuation* equation that allows us to calculate the gravitational acceleration anywhere in free space from a knowledge of its values over the surface. Upward continuation is effectively smoothing. Although upward continuation is not done much in gravity analysis, it is used in magnetic interpretation to compare measurements made at different flight elevations.

If we can calculate the gravity field over a surface closer to the anomaly sources, the anomaly should be sharper and less confused by the effects of deeper features. This process, called *downward continuation*, was described by Peters (1949). It involves calculating a gravity value at depth from gravity values and derivatives on a shallower surface. The derivatives are usually evaluated by averaging over circles of different radii as described in Section 2.6.5. The main theoretical limitation on the method is singularities associated with masses through which the continuation process is carried. The main practical limitation is imposed by uncertainty in the measured field; because derivatives involve differences, their calculation magnifies uncertainties. The result is that minor noise is increased in the downward-continued field and this noise may outweigh the benefits of sharpening anomalies.

We begin with Laplace's equation (2.11b) (thus implicitly assuming that we will not continue through any masses) and the expressions for second derivatives calculated by finite differences [Eq. (2.45)]. For the point  $(x_0, y_0, 0)$  and station spacing  $s$ , we write

$$\begin{aligned}\partial^2 g / \partial x^2 &= \{ g(x_0 + s, y_0, 0) - 2g(x_0, y_0, 0) \\ &\quad + g(x_0 - s, y_0, 0) \} / s^2 \\ \partial^2 g / \partial y^2 &= \{ g(x_0, y_0 + s, 0) - 2g(x_0, y_0, 0) \\ &\quad + g(x_0, y_0 - s, 0) \} / s^2 \\ \partial^2 g / \partial z^2 &= \{ g(x_0, y_0, +s) - 2g(x_0, y_0, 0) \\ &\quad + g(x_0, y_0, -s) \} / s^2\end{aligned}$$

If we take  $z$  to be positive downward, then  $g(x_0, y_0, +s)$  is the gravity value a distance  $s$  below the station  $g(x_0, y_0, 0)$ . Substituting into Laplace's

equation, we get

$$\begin{aligned}g(x_0, y_0, +s) &= 6g(x_0, y_0, 0) \\ &\quad - \{ g(x_0 + s, y_0, 0) \\ &\quad + g(x_0 - s, y_0, 0) \\ &\quad + g(x_0, y_0 + s, 0) \\ &\quad + g(x_0, y_0 - s, 0) \\ &\quad + g(x_0, y_0, -s) \} \quad (2.49)\end{aligned}$$

All of these terms can be found from the gravity values read from a grid except for the last term, which can be found from Equation (2.48). Similar but more complicated procedures use concentric circles passing through grid stations. Other methods employ Fourier transform theory (see Grant and West, 1965, p. 218).

## 2.7. GRAVITY INTERPRETATION

### 2.7.1. General

After the camouflaging interference effects of other features have been removed to the best of our ability, the interpretation problem usually is finding the mass distribution responsible for the residual anomaly. This often is done by *iterative modeling* (Bhattacharyya, 1978). The field of a model mass distribution is calculated and subtracted from the residual anomaly to determine the effects for which the model cannot account. Then the model is changed and the calculations repeated until the remaining effects become smaller than some value considered to be "close enough." To limit the number of possible changes, we include some predetermined constraints, for example, we might change only the upper surface of the mass distribution.

Before iterative modeling became practical, interpreters generally compared residual anomalies to anomalies associated with simple shapes, and this procedure is still useful in many situations. Simple shapes can be modeled with a microcomputer (Reeves and MacLeod, 1983). A gravity anomaly is not especially sensitive to minor variations in the shape of the anomalous mass, so that simple shapes often yield results that are close enough to be useful. Study of the gravity effect of simple shapes also helps in understanding the types of information that can be

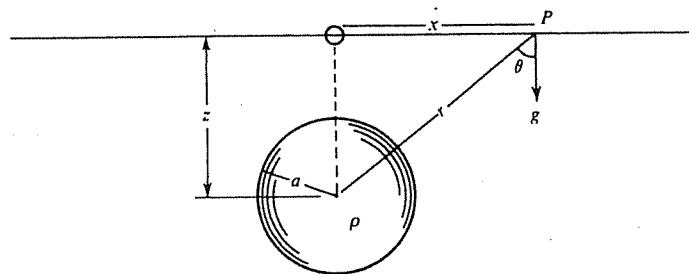
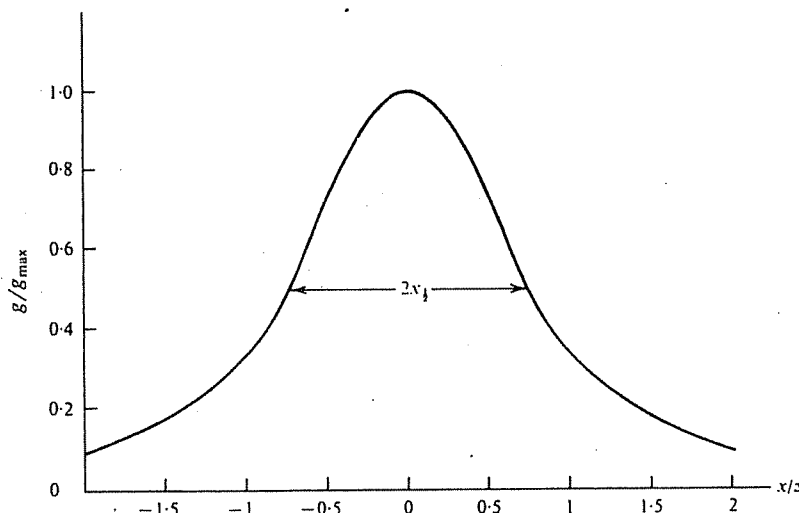


Figure 2.23. Gravity effect of a sphere.

learned, for example, in determining what aspects of an anomaly indicate the depth, shape, density contrast, total mass, and so forth.

In the following examples, the density symbol  $\rho$  is the density contrast with respect to the laterally equivalent material (in numerical relations,  $\rho$  is the difference in specific gravity because density is usually given in grams per cubic centimeters even where linear dimensions are given in English units).

### 2.7.2. Gravity Effect of a Sphere

The gravity effect of a sphere at a point  $P$  (Fig. 2.23), directed along  $r$ , is  $g_r = \gamma M/r^2$ . The vertical component is

$$g = g_r \cos \theta = \gamma M z / r^3$$

$$= k \rho a^3 z / (x^2 + z^2)^{3/2} \text{ mGal} \quad (2.50)$$

where

$$k = 4\pi \gamma / 3$$

$= 27.9 \times 10^{-3}$  when  $a, x, z$  are in meters

$= 8.52 \times 10^{-3}$  when  $a, x, z$  are in feet

Note that  $z$  is the depth to the sphere center rather than to the top of the sphere and that the profile is symmetrical about the origin taken directly above the center. The maximum value of  $g$  is

$$g_{\max} = 27.9 \times 10^{-3} \rho a^3 / z^2 \text{ when } a, z \text{ in meters} \quad (2.51a)$$

$$= 8.52 \times 10^{-3} \rho a^3 / z^2 \text{ when } a, z \text{ in feet} \quad (2.51b)$$

The depth of the center of the sphere,  $z$ , can be found from a profile. When  $g = g_{\max}/2$ ,  $z = 1.3x_{1/2}$ ,

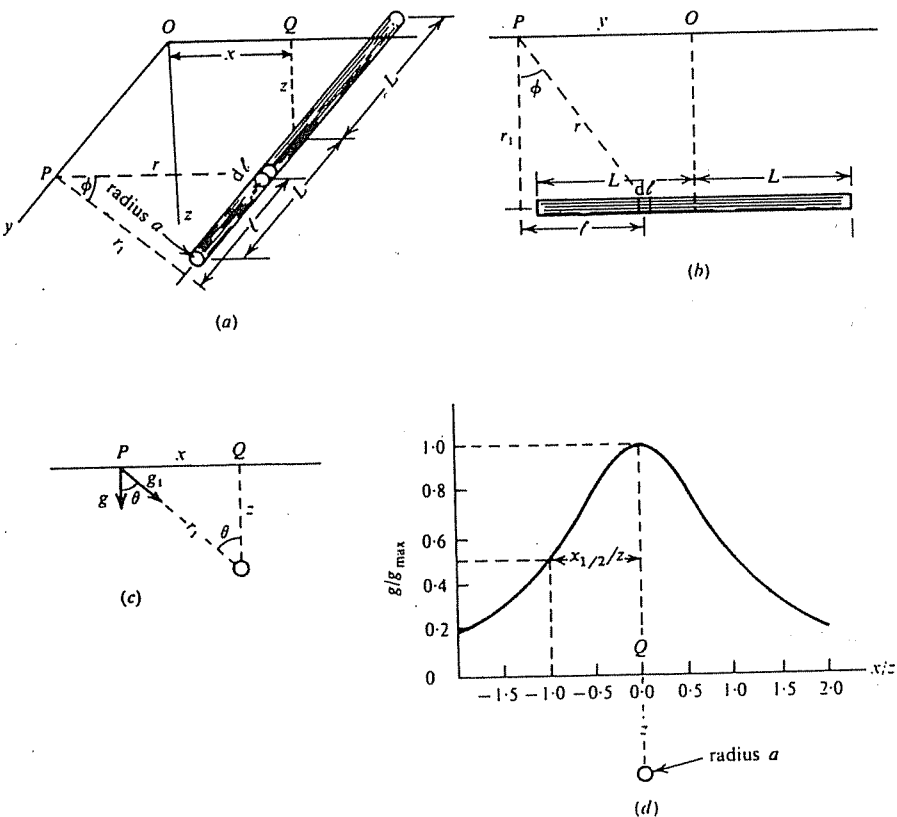


Figure 2.24. Gravity effect of a horizontal rod. (a) Three-dimensional view. (b) Projection on the plane containing the rod and the  $y$  axis. (c) Projection on the  $xz$  plane. (d) Gravity profile along the  $x$  axis ( $L = \infty$ ).

where  $x_{1/2}$  is the half-width of the profile, that is, half the width at the half-maximum value. We can also express the mass of the sphere,  $M$ , in terms of  $x_{1/2}$  and  $g_{\max}$ :

$$M = 25.5 g_{\max} (x_{1/2})^2 \text{ tonnes} \quad (2.52a)$$

where  $x_{1/2}$  is in meters, or, where  $x'_{1/2}$  is in feet,

$$M = 2.61 g_{\max} (x'_{1/2})^2 \text{ short tons} \quad (2.52b)$$

The spherical shape is particularly useful as a first approximation in the interpretation of three-dimensional anomalies that are approximately symmetrical.

### 2.7.3. Gravity Effect of a Horizontal Rod

The effect at  $P(x, y, 0)$  of a segment of length  $dl$  of a horizontal rod perpendicular to the  $x$  axis at a depth  $z$  (Fig. 2.24) with mass  $m$  per unit length is

$$dg_r = \gamma m dl / r^2 = \gamma m (r_1 d\phi / \cos^2 \phi) / r^2 = \gamma m d\phi / r_1$$

where  $dl = (r_1 d\phi / \cos^2 \phi)$ . The component along  $r_1$

is

$$dg_1 = dg_r \cos \phi = \gamma m \cos \phi d\phi / r_1$$

and the vertical component is

$$dg = dg_1 \cos \theta = dg_1 (z/r_1) = \gamma m z \cos \phi d\phi / r_1^2$$

Integrating from  $\tan^{-1}((y - L)/r_1)$  to  $\tan^{-1}((y + L)/r_1)$ , we get

$$\begin{aligned} g &= \left( \frac{\gamma m z}{r_1^2} \right) \left[ \frac{y + L}{\{(y + L)^2 + r_1^2\}^{1/2}} \right. \\ &\quad \left. - \frac{y - L}{\{(y - L)^2 + r_1^2\}^{1/2}} \right] \\ &= \frac{\gamma m}{z(1 + x^2/z^2)} \left[ \frac{1}{\{1 + (x^2 + z^2)/(y + L)^2\}^{1/2}} \right. \\ &\quad \left. - \frac{1}{\{1 + (x^2 + z^2)/(y - L)^2\}^{1/2}} \right] \quad (2.53) \end{aligned}$$

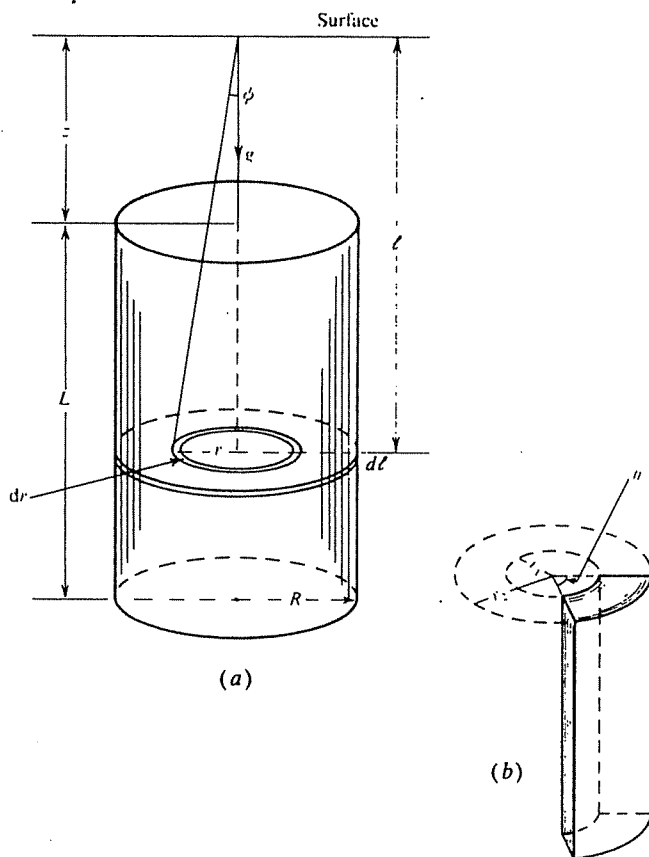


Figure 2.25. Gravity effect of a vertical cylinder. (a) Calculation of gravity over the axis.  
(b) Geometry of a cylindrical slice.

If the rod is infinite in length, the limits of integration would have been  $\pm \pi/2$  and the result would be

$$g = 2\gamma m/z(1 + x^2/z^2) \quad (2.54)$$

This is usually a good approximation when  $L > 10z$ . The depth  $z$  to the center of the rod in Equation (2.54) can be found from the half-width  $x_{1/2}$ :

$$z = x_{1/2} \quad (2.55)$$

If the rod is expanded into a cylinder of radius  $a$ , the only change in Equations (2.53) and (2.54) is that  $m = \pi a^2 \rho$ .

#### 2.7.4. Gravity Effect of a Vertical Cylinder

The gravity effect on the axis of a vertical cylinder (which is the maximum value) can easily be calculated. First we find  $g$  on the axis for a disk of thickness  $d\ell$  (Fig. 2.25a). We start with an elementary ring of width  $dr$  whose mass is  $\delta m = 2\pi\rho r dr d\ell$ ,

so that its gravity effect is

$$\begin{aligned} \delta g &= \gamma \delta m \cos \phi / (r^2 + \ell^2) \\ &= (2\pi\rho\gamma d\ell) r dr \cos \phi / (r^2 + \ell^2) \\ &= 2\pi\gamma\rho d\ell \sin \phi d\phi \end{aligned}$$

on eliminating  $r$ . Integrating first from  $\phi = 0$  to  $\tan^{-1}(R/\ell)$  for the disk and then from  $\ell = z$  to  $z + L$ , we get, for the whole cylinder,

$$\begin{aligned} g &= 2\pi\gamma\rho \int_z^{z+L} \left\{ 1 - \ell / (\ell^2 + R^2)^{1/2} \right\} d\ell \\ &= 2\pi\gamma\rho \left[ L + (z^2 + R^2)^{1/2} \right. \\ &\quad \left. - \left\{ (z + L)^2 + R^2 \right\}^{1/2} \right] \quad (2.56) \end{aligned}$$

where

$$\begin{aligned} 2\pi\gamma &= 41.9 \times 10^{-3} \quad \text{when } z, R, L \text{ are in meters} \\ &= 12.77 \times 10^{-3} \quad \text{when } z, R, L \text{ are in feet} \end{aligned}$$

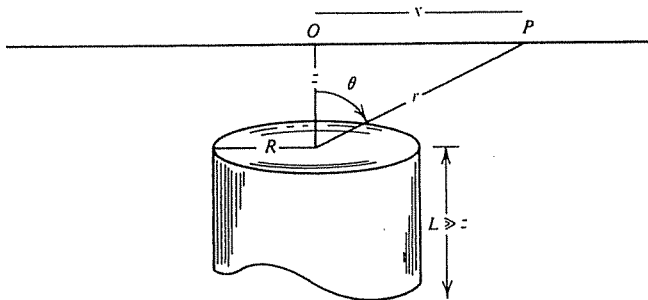
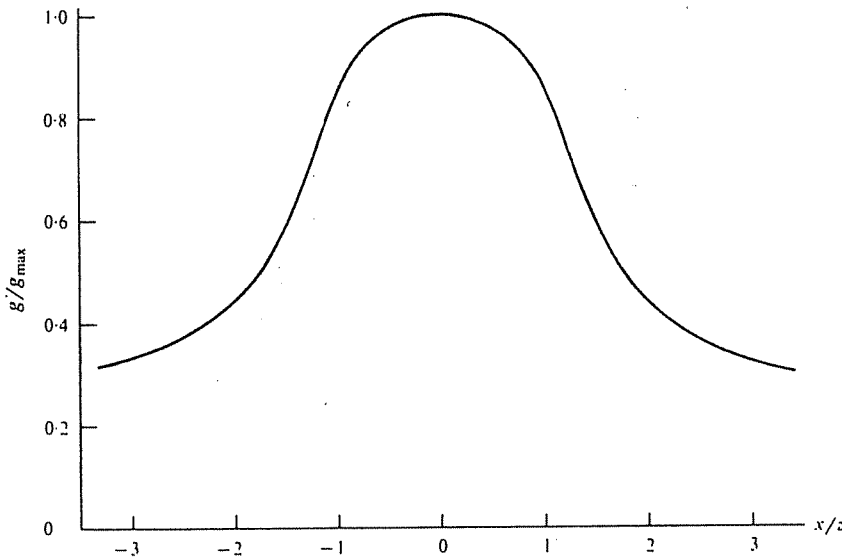


Figure 2.26. Gravity effect off the axis of a vertical cylinder.

There are several cases of special significance:

1. If  $R \rightarrow \infty$ , we have an infinite horizontal slab and

$$g = 2\pi\gamma\rho L \quad (2.57)$$

This is the Bouguer correction given in Section 2.3.2d. Note that  $g$  is independent of the depth of the slab and varies only with its thickness.

2. The terrain correction can be obtained using a sector of the cylinder as shown in Figure 2.25b. We have  $\delta m = \rho(r\theta) dr d\ell$  so that

$$\begin{aligned} \delta g &= \gamma(\rho r\theta dr d\ell) \cos\phi / (r^2 + \ell^2) \\ &= \gamma\rho\theta d\ell \sin\phi d\phi \end{aligned}$$

on eliminating  $r$ . We integrate from  $\phi = \tan^{-1}(r_1/\ell)$  to  $\tan^{-1}(r_2/\ell)$  and from  $\ell = 0$  to  $L$ .

The result is

$$\delta g_T = \gamma\rho\theta \left\{ (r_2 - r_1) + (r_1^2 + L^2)^{1/2} - (r_2^2 + L^2)^{1/2} \right\} \quad (2.58)$$

which is Equation (2.26) with  $L$  replacing  $\Delta z$ .

3. When  $z = 0$ , the cylinder outcrops and we get

$$g = 2\pi\gamma\rho \left\{ L + R - (L^2 + R^2)^{1/2} \right\} \quad (2.59)$$

4. If  $L \rightarrow \infty$ , we have

$$g = 2\pi\gamma\rho \left\{ (z^2 + R^2)^{1/2} - z \right\} \quad (2.60)$$

If, in addition,  $z = 0$ , we have

$$g = 2\pi\gamma\rho R \quad (2.61)$$

When  $L \gg z$ , we can use Equation (2.60) to get the gravity off-axis (see MacRobert, 1948:151–5 or Pipes and Harvill, 1970:348–9). Because  $g$  satisfies Laplace's equation, we can express it in a series of

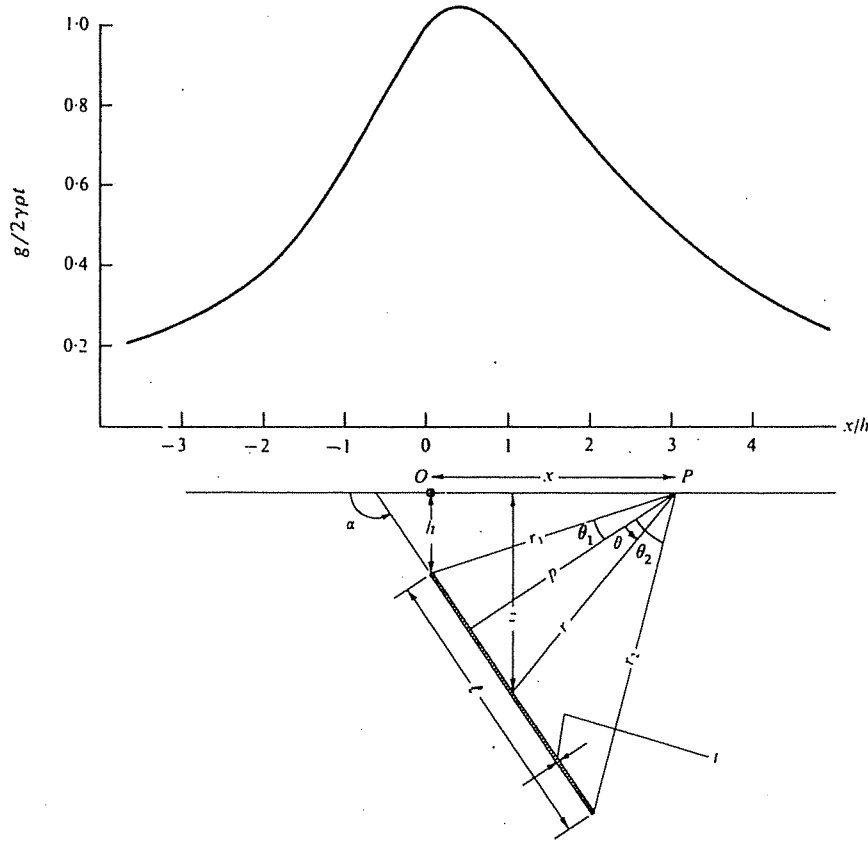


Figure 2.27. Gravity effect of a thin sheet of infinite strike length.

Legendre polynomials  $P_n(\mu)$  where  $\mu = \cos \theta$  (Pipes and Harvill, 1970:799–805). Taking  $r > z$  in Figure 2.26, we have three cases to consider:  $r > z > R$ ,  $R > r > z$ , and  $r > R > z$ . For the first case, we get (see problem 3)

$$g(r, \theta) = 2\pi\gamma\rho R \left\{ (R/2r) - (R/2r)^3 P_2(\mu) + 2(R/2r)^5 P_4(\mu) - \dots \right\} \quad (2.62)$$

For the second case,  $R > r > z$ , the result is

$$g(r, \theta) = 2\pi\gamma\rho R \left\{ 1 - 2(r/2R) P_1(\mu) + 2(r/2R)^2 P_2(\mu) - 2(r/2R)^4 P_4(\mu) + \dots \right\} \quad (2.63)$$

The result for the third case,  $r > R > z$ , is the same as Equation (2.62), showing that Equation (2.62) is valid whenever  $r > R$ . From Equations (2.62) and (2.63) we get the curve in Figure 2.26.

### 2.7.5. Gravity Effect of a Thin Dipping Sheet

Considerable simplification can be effected when a body can be considered two-dimensional. In general,

this holds when the strike length is about 20 times the other dimensions (including depth).

Referring to Figure 2.27, we have the following relations:

$$\begin{aligned} p &= (x - h \cot \alpha) \sin \alpha = x \sin \alpha - h \cos \alpha, \\ r &= p \sec \theta \\ z &= r \sin(\alpha + \theta - \pi/2) = p(\sin \alpha \tan \theta - \cos \alpha) \\ dz &= p \sin \alpha \sec^2 \theta d\theta \\ r_1 &= (x^2 + h^2)^{1/2}, \\ r_2 &= \{(x + \ell \cos \alpha)^2 + (h + \ell \sin \alpha)^2\}^{1/2} \end{aligned}$$

Now we apply Equation (2.9) for a two-dimensional structure. The product  $dx dz$  in Equation (2.9) represents an element of area of the cross section, that is,

$$dx dz = t d\ell = t \csc \alpha dz = t p \sec^2 \theta d\theta$$

Equation (2.9) now gives (note that  $r'$  is the same as

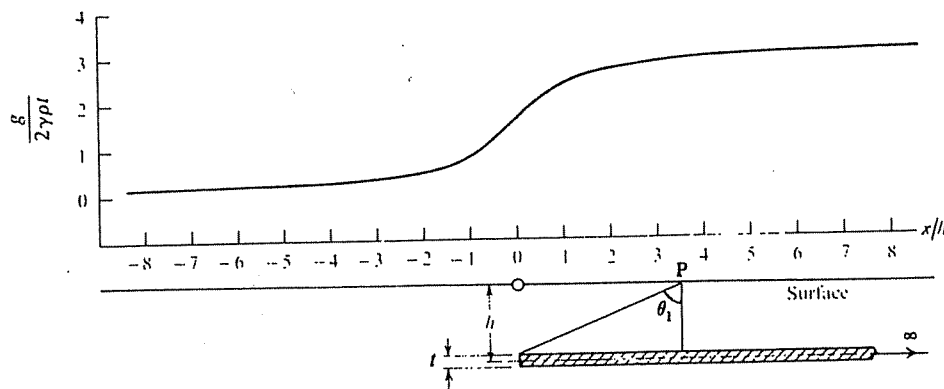


Figure 2.28. Gravity effect of a semiinfinite horizontal sheet.

$r$  here)

$$\begin{aligned}
 g &= 2\gamma\rho t p \int_{-\theta_1}^{\theta_2} (z/r^2) \sec^2 \theta \, d\theta \\
 &= 2\gamma\rho t \int_{-\theta_1}^{\theta_2} (\sin \alpha \tan \theta - \cos \alpha) \, d\theta \\
 &= 2\gamma\rho t \{ \sin \alpha \ln(\cos \theta_1 / \cos \theta_2) - (\theta_2 + \theta_1) \cos \alpha \} \\
 &= 2\gamma\rho t \{ \sin \alpha \ln(r_2/r_1) - (\theta_2 + \theta_1) \cos \alpha \}
 \end{aligned} \quad (2.64)$$

If the sheet is vertical, Equation (2.64) simplifies to

$$g = 2\gamma\rho t \ln[(h + \ell)^2 + x^2]/(x^2 + h^2) \quad (2.65)$$

The thin sheet is a good approximation to a prism unless the thickness of the prism is somewhat greater than  $h$ , the depth to the top. When the dip is steep ( $> 60^\circ$ ), the depth can be roughly estimated from the half-width, for example, when  $h \approx \ell$ ,  $h \approx 0.7x_{1/2}$ . However, when  $\ell$  is large or when the dip is small it is not possible to get a reliable estimate.

### 2.7.6. Gravity Effect of Horizontal Sheets, Slabs, Dikes, and Faults

(a) *Horizontal thin sheet.* When the sheet in Equation (2.64) is horizontal,  $\alpha = \pi$  and we have

$$\begin{aligned}
 g &= 2\gamma\rho t(\theta_1 + \theta_2) \\
 &= 2\gamma\rho t [\tan^{-1}\{(\ell - x)/h\} + \tan^{-1}(x/h)]
 \end{aligned} \quad (2.66)$$

If, in addition,  $\ell \rightarrow \infty$ , we have, for a semiinfinite

horizontal sheet,

$$g = 2\gamma\rho t \{ \pi/2 + \tan^{-1}(x/h) \} \quad (2.67)$$

and if the sheet extends to infinity in the other direction (that is,  $x$  goes to infinity as well) we have the Bouguer correction as in Equation (2.57) with  $t$  replacing  $L$ .

The profile for a semiinfinite horizontal sheet is shown in Figure 2.28. The thin sheet result can be used to approximate a horizontal slab with an error less than 2% when  $h > 2t$ . A fault often can be approximated by two semiinfinite horizontal sheets, one displaced above the other as in Figure 2.29.

(b) *Horizontal slab.* Equation (2.67) can be used to find the gravity effect of a semiinfinite horizontal slab terminating at a plane dipping at the angle  $\alpha$  (Fig. 2.30). We use Equation (2.67) to get the effect of the thin sheet of thickness  $dz$  and then integrate to find the result for the slab (Geldart, Gill, and Sharma, 1966).

We must replace  $x$  in Equation (2.67) with  $(x + z \tan \beta)$ , so  $\tan^{-1}(x/h)$  becomes  $\tan^{-1}\{(x + z \tan \beta)/z\} = \theta$ . Equation (2.67) now gives

$$g = 2\gamma\rho \int_{z_1}^{z_2} (\pi/2 + \theta) \, dz = 2\gamma\rho \left( \pi t/2 + \int_{z_1}^{z_2} \theta \, dz \right)$$

We now have:

$$\begin{aligned}
 \tan \theta &= (x + z \tan \beta)/z = (x/z) + \tan \beta \\
 z &= x/(\tan \theta - \tan \beta) \\
 dz &= -x \sec^2 \theta \, d\theta / (\tan \theta - \tan \beta)^2 \\
 &= -x \cos^2 \beta \, d\theta / \sin^2(\theta - \beta) \\
 &= -x \cos^2 \beta \, d\psi / \sin^2 \psi
 \end{aligned}$$

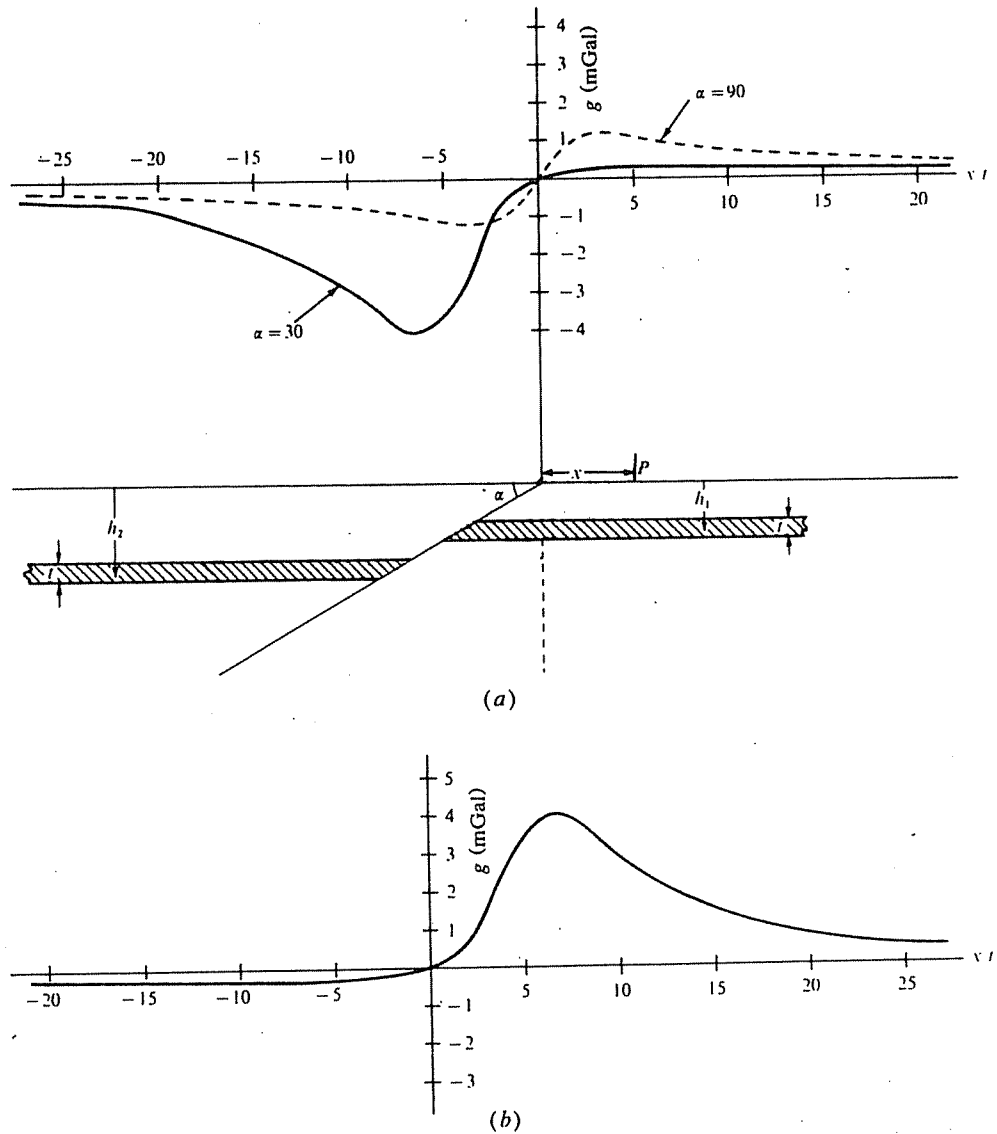


Figure 2.29. Gravity effect of a faulted horizontal sheet;  $t = 300$  m,  $h_1 = 750$  m,  $h_2 = 1350$  m, and  $\rho = 1 \text{ g/cm}^3$ . (a) Normal fault dipping  $\alpha = 30$  and  $90^\circ$ . (b) Reverse fault,  $\alpha = -30^\circ$ .

where  $\psi = \theta - \beta$ . Substituting for  $dz$ , we get

$$g = 2\gamma\rho \left\{ \pi t/2 - x \cos^2 \beta \int_{\psi_1}^{\psi_2} (\psi + \beta) d\psi / \sin^2 \psi \right\}$$

Using the relation  $\int dx / \sin^2 x = -\cot x$ , we can integrate the first term by parts, that is,

$$\begin{aligned} \int \psi d\psi / \sin^2 \psi &= -\psi \cot \psi + \int \cot \psi d\psi \\ &= -\psi \cot \psi + \ln(\sin \psi) \end{aligned}$$

Thus,

$$g = 2\gamma\rho \left[ \pi t/2 - x \cos^2 \beta \{ -\psi \cot \psi + \ln(\sin \psi) - \beta \cot \psi \} \Big|_{\psi_1}^{\psi_2} \right]$$

$$= 2\gamma\rho \left[ \pi t/2 + x \cos^2 \beta \{ (\psi_2 + \beta) \cot \psi_2 - (\psi_1 + \beta) \cot \psi_1 - \ln(\sin \psi_2 / \sin \psi_1) \} \Big|_{\psi_1}^{\psi_2} \right]$$

$$= 2\gamma\rho \left[ \pi t/2 + x \cos^2 \beta \{ (\psi_2 + \beta) \cot \psi_2 - (\psi_1 + \beta) \cot \psi_1 - \ln(\sin \psi_2 / \sin \psi_1) \} \right]$$

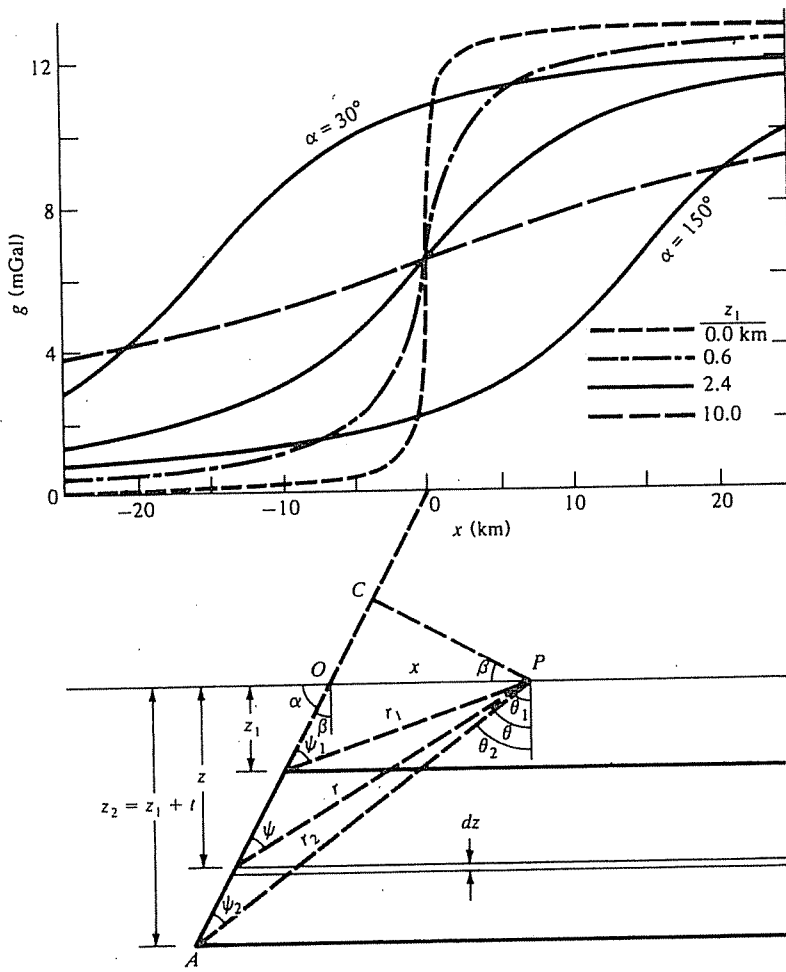


Figure 2.30. Gravity effect of a semiinfinite slab.  $t = 300 \text{ m}$ ,  $\alpha = 90^\circ$  except where otherwise noted on the curves,  $\rho = 1 \text{ gm/cm}^3$ .

Figure 2.30 shows that

so

$$\begin{aligned}\beta(\cot \psi_2 - \cot \psi_1) &= \beta(AC/CP - BC/CP) \\ &= \beta(AB/CP) \\ &= \beta(t/\cos \beta)/(x \cos \beta) \\ &= \beta t/(x \cos^2 \beta)\end{aligned}$$

$$(\sin \psi_2 / \sin \psi_1) = r_1/r_2$$

Also,

$$\begin{aligned}\cot \psi_i &= \{(z_i/\cos \beta) + x \sin \beta\}/x \cos \beta \\ &= (z_i + x \sin \beta \cos \beta)/x \cos^2 \beta\end{aligned}$$

so that we finally get

$$g = 2\gamma\rho \left\{ (\pi/2 + \beta)t + x \cos^2 \beta (F_2 - F_1) \right\} \quad (2.68)$$

Substituting in Equation (2.68) and noting that  $t = (z_2 - z_1)$ , we obtain

$$\begin{aligned}g &= 2\gamma\rho \left\{ (\pi/2 + \beta)t + (\theta_2 - \beta) \right. \\ &\quad \times (z_2 + x \sin \beta \cos \beta) \\ &\quad - (\theta_1 - \beta)(z_1 + x \sin \beta \cos \beta) \\ &\quad \left. + x \cos^2 \beta \ln(r_2/r_1) \right\} \\ &= 2\gamma\rho \left\{ (\pi t/2) + (z_2\theta_2 - z_1\theta_1) \right. \\ &\quad + x(\theta_2 - \theta_1) \sin \beta \cos \beta \\ &\quad \left. + x \cos^2 \beta \ln(r_2/r_1) \right\} \quad (2.69)\end{aligned}$$

where

$$\begin{aligned}F_i &= \psi_i \cot \psi_i - \ln(\sin \psi_i) \quad \psi_i = \theta_i - \beta \\ \theta_i &= \tan^{-1}\{(x/z_i) + \tan \beta\}\end{aligned}$$

Equation (2.68) is sometimes given in another form. From Figure 2.30 we have

$$\begin{aligned}x/\sin \psi_1 &= r_1/\sin(\pi/2 + \beta) = r_1/\cos \beta \\ x/\sin \psi_2 &= r_2/\cos \beta\end{aligned}$$

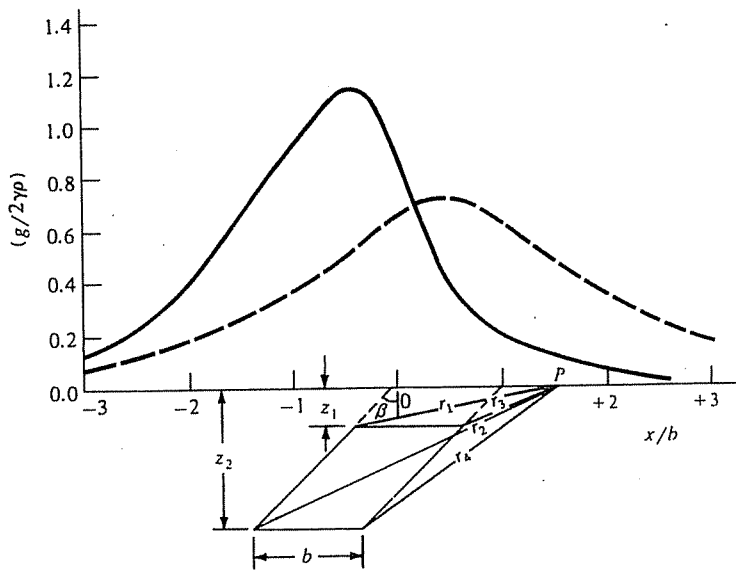


Figure 2.31. Gravity effect of a dike. Profiles are perpendicular to the dike.  $L = \infty$ ,  $b = 1$ ,  $z_1 = 1/3$ ,  $z_2 = 4/3$ ,  $\beta = 45^\circ$  (solid line),  $0^\circ$  (dashed line).

If the end of the slab is vertical,  $\beta = 0$  and this is  
Equation (2.69) gives

$$g = 2\gamma\rho \{ (\pi t/2) + (z_2\theta_2 - z_1\theta_1) + x \ln(r_2/r_1) \} \quad (2.70)$$

If the slab outcrops,  $z_1 = 0$ ,  $z_2 = t$ ,  $\theta_1 = \pi/2$ ,  $r_1 = x$ , and

$$g = 2\gamma\rho \{ (\pi t/2) + \theta_2 t + x(\theta_2 - \pi/2)\sin\beta\cos\beta + x\cos^2\beta\ln(r_2/x) \} \quad (2.71)$$

Figure 2.30 shows curves for a semiinfinite slab. The slope is quite sensitive to the depth of the slab but not to the dip of the end.

(c) Thick two-dimensional dike. The result for the dike in Figure 2.31 can be obtained by subtracting two slabs, one being displaced horizontally with respect to the other. The result is

$$g = 2\gamma\rho \cos^2\beta \{ x(F_2 - F_1) - (x - b)(F_4 - F_3) \} \quad (2.72)$$

using Equation (2.68). In terms of Equation (2.69),

$$\begin{aligned} g &= 2\gamma\rho [ z_2(\theta_2 - \theta_4) - z_1(\theta_1 - \theta_3) \\ &\quad + \sin\beta\cos\beta \{ x(\theta_2 - \theta_1) \\ &\quad - (x - b)(\theta_4 - \theta_3) \} \\ &\quad + \cos^2\beta \{ x\ln(r_2/r_1) \\ &\quad - (x - b)\ln(r_4/r_3) \}] \\ &= 2\gamma\rho [ z_2(\theta_2 - \theta_4) - z_1(\theta_1 - \theta_3) \\ &\quad + \sin\beta\cos\beta \{ x(\theta_2 + \theta_3 - \theta_4 - \theta_1) \\ &\quad + b(\theta_4 - \theta_3) \} \\ &\quad + \cos^2\beta \{ x\ln(r_2r_3/r_4r_1) \\ &\quad + b\ln(r_4/r_3) \}] \end{aligned} \quad (2.73)$$

When the sides of the dike are vertical,  $\beta = 0$  and

$$g = 2\gamma\rho \{ z_2(\theta_2 - \theta_4) - z_1(\theta_1 - \theta_3) + x\ln(r_2r_3/r_4r_1) + b\ln(r_4/r_3) \} \quad (2.74)$$

If the dike outcrops,  $z_1 = 0$ ,  $r_1 = x$ ,  $r_3 = (x - b)$ ,  $\theta_1 = \pi/2 = \theta_3$ , and the result is

$$\begin{aligned} g &= 2\gamma\rho [ z_2(\theta_2 - \theta_4) + \sin\beta\cos\beta \\ &\quad \times \{ x(\theta_2 - \theta_4) - b(\pi/2 - \theta_4) \} \\ &\quad + x\cos^2\beta\ln\{ r_2(x - b)/r_4x \} \\ &\quad + b\cos^2\beta\ln\{ r_4/(x - b) \} ] \end{aligned} \quad (2.75)$$

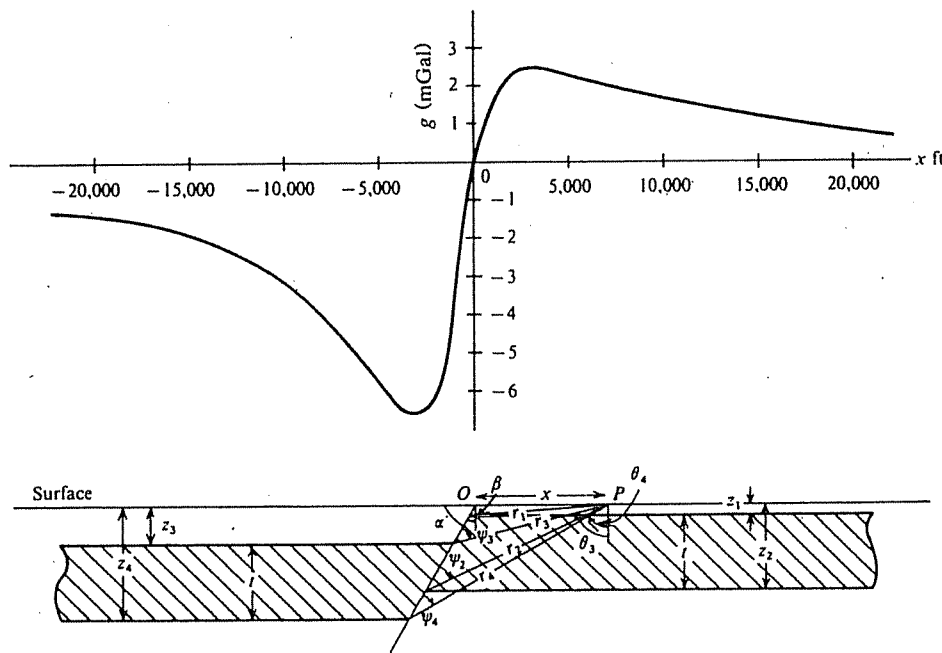


Figure 2.32. Gravity effect of a faulted horizontal bed;  $t = 1,200$  m,  $z_1 = 150$  m,  $z_2 = 1,350$  m,  $z_3 = 600$  m,  $z_4 = 1,800$  m,  $\alpha = 60^\circ$ , and  $\rho = 1 \text{ g/cm}^3$ . (From Geldart, Gill, and Sharma, 1966.)

If the dike is also vertical, this reduces further to

$$g = 2\gamma\rho [z_2(\theta_2 - \theta_1) + x \ln\{r_2(x-b)/r_4x\} + b \ln\{r_4/(x-b)\}] \quad (2.76)$$

An estimate of  $z_1$ , the depth to the top of the dike, is not very satisfactory in terms of  $x_{1/2}$ . When  $z_1 = b$ , we find that  $z_1 = 0.67x_{1/2}$  when  $z_2 = 2b$ , and  $z_1 = 0.33x_{1/2}$  when  $z_2 = 10b$ , that is, a factor of 2 depending on the depth extent. In general, the curves become sharper as both  $z_1$  and  $z_2$  get smaller. Also, it is impossible to make a good estimate of the width of the dike from the shape of the curve.

(d) Fault. The gravity effect of the fault shown in Figure 2.32 can be obtained by adding the effects of:

- (i) A near-surface semiinfinite slab.
- (ii) A deeper infinite slab of the same thickness.
- (iii) A semiinfinite slab of negative density contrast to wipe out the part of the infinite slab under the near-surface slab.

The result is

$$g = 2\gamma\rho [\pi t + x \cos^2 \beta \{(F_2 - F_1) - (F_4 - F_3)\}] \quad (2.77)$$

A typical curve is shown in Figure 2.32 (note that the

constant term  $2\pi\gamma\rho t$  has been omitted). Obviously one can extend Equation (2.77) to include a series of horizontal beds at increasing depths.

### 2.7.7. Applying Simple Models to Actual Anomalies

Most of the formulas for simple shapes are far from easy to apply. Even when we can assume that a field result can be matched by a specific geometry, it is still tedious to plot profiles from expressions that contain a number of geometrical unknowns in addition to the density contrast. Use of a collection of characteristic curves reduces the labor involved.

We first establish some significant features associated with the profiles. Usually the number of parameters is reduced by measuring in terms of one of them, preferably the one that influences the significant features the least. Grant and West (1965, pp. 273–80) discussed how to construct curves for the thin dipping sheet model. They concluded that symmetry and sharpness are the most diagnostic features, and thus they developed curves in terms of ratios that depend principally on these properties.

### 2.7.8. Gravity Effects of Complex Shapes

The gravity effects of complex shapes are usually calculated by subdividing the body into rectangular cells, calculating the effect of each with a digital

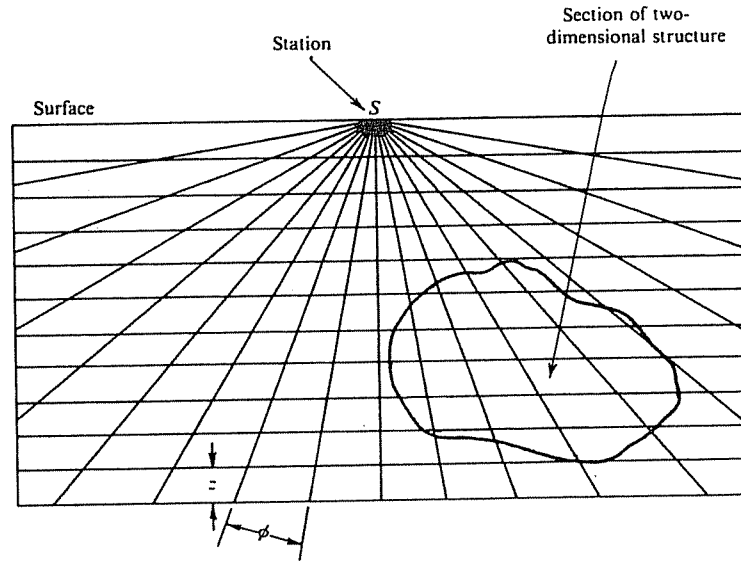


Figure 2.33. Template for calculating the gravity effect of two-dimensional bodies of irregular cross section. (From Hubbert, 1948).

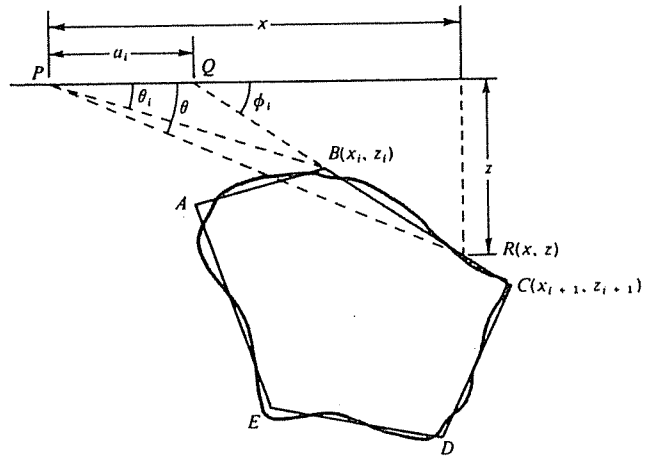


Figure 2.34. Polygon approximation of an irregular vertical section of a two-dimensional body.

computer, and then summing. This procedure is sometimes carried out graphically using templates superimposed on a cross section to divide it into elementary areas, each of which contributes the same effect at a surface station.

A template of this type is shown in Figure 2.33. The gravity effect at the chart apex is

$$g \approx K \times 10^{-5} N \phi z \text{ mGal} \quad (2.78)$$

where  $N$  is the number of segments covering the cross section,  $\phi$  is the angular separation of radial lines,  $z$  is the separation of horizontal lines,  $K = 23$  for  $z$  in meters and 7.1 for  $z$  in feet.

When the structure is not really two dimensional, the finite length can be taken into account by applying a correction. For a point in the plane of the cross section of a finite structure at a distance  $r$  from the section's center of gravity, the correction is

$$\frac{g}{g_m} = \frac{1}{2} \left\{ \frac{1}{(1 + r^2/Y_1^2)^{1/2}} + \frac{1}{(1 + r^2/Y_2^2)^{1/2}} \right\} \quad (2.79)$$

where  $g$  is the actual gravity of the finite body,  $g_m$  is the gravity for a body of the same cross section and of infinite length, and  $Y_1, Y_2$  are the distances from the cross section to the ends of the body.

Graphical methods have also been employed on three-dimensional bodies by placing templates over

contours of the body in a horizontal plane. In effect, the body is broken up into a stack of horizontal slabs whose thickness is determined by the contour interval. This approach is more difficult than the two-dimensional procedure because the chart must have a variable scale parameter to allow for different slab depths.

One can calculate the gravity effect of a 2-D body of arbitrary cross section by using an  $n$ -sided polygon to approximate the outline of the vertical section (Talwani, Worzel, and Landisman, 1959). A simple section is illustrated in Figure 2.34. The gravity effect of this section is equal to a line integral around the perimeter (Hubbert, 1948). The relation is

$$g = 2\gamma\rho \oint z d\theta$$

From the geometry of Figure 2.34 we have the following relations:

$$z = x \tan \theta = (x - a_i) \tan \phi_i$$

or

$$z = (a_i \tan \theta \tan \phi_i) / (\tan \phi_i - \tan \theta)$$

The line integral for the side  $BC$  is

$$\int_{BC} z d\theta = \int_B^C \frac{a_i \tan \theta \tan \phi_i}{\tan \phi_i - \tan \theta} d\theta = Z_i$$

Thus,

$$g = 2\gamma\rho \sum_{i=1}^n Z_i \quad (2.80)$$

In the most general case,  $Z_i$  is given by

$$Z_i = a_i \sin \phi_i \cos \phi_i \left[ (\theta_i - \theta_{i+1}) + \tan \phi_i \cdot \ln \left( \frac{\cos \theta_i (\tan \theta_i - \tan \phi_i)}{\cos \theta_{i+1} (\tan \theta_{i+1} - \tan \phi_i)} \right) \right] \quad (2.81)$$

where

$$\theta_i = \tan^{-1} \left( \frac{z_i}{x_i} \right), \quad \phi_i = \tan^{-1} \left( \frac{z_{i+1} - z_i}{x_{i+1} - x_i} \right)$$

$$a_i = x_{i+1} - z_{i+1} \cot \phi_i \\ = x_{i+1} + z_{i+1} \left( \frac{x_{i+1} - x_i}{z_i - z_{i+1}} \right)$$

This technique has also been used for three-dimensional bodies by replacing the contours in the horizontal plane with  $n$ -sided polygons. The solution, from line integrals of the polygons, is essentially a more complicated version of Equation (2.81).

### 2.7.9. The Direct and Inverse Problems of Interpretation

The interpretation techniques outlined in previous sections employ models with simplified shapes. Calculating the effects of models is the *direct* or *forward approach* to interpretation (the same procedure is used in other geophysical methods). The initial selection of a reasonable model is made with the aid of geological information and the experience of the interpreter. Interpretation in terms of simple models, a more-or-less force-fit to the data, is commonly used when data and control are incomplete. Detailed analysis is complicated by the fact that model fits are not unique. Ambiguity is well illustrated in the classic paper of Skeels (1947), who shows a gravity profile that could be produced by a number of mass distributions.

The inverse problem involves determining the geometry and physical properties of the source from measurements of the anomaly, rather than simply selecting a model and determining the parameters that match the anomaly approximately. The inherent nonuniqueness may make such a task appear to be a waste of time; however, with additional constraints and a computer, this type of analysis becomes increasingly useful.

We outline here a typical least-squares procedure for the inverse method. First, assume some mathematical model based on prior knowledge of the geology and/or of the geometry plus additional information gleaned from the general appearance of profiles and contours. Next, limit the number of parameters allowed to vary, for example, some subset of strike, length, attitude, depth, and depth extent; this makes the inverse problem more tractable. Next, linearize the problem (because the mathematical model is often essentially nonlinear) to simplify computations. Matrices (§A.2) are generally used. The solution is obtained by using the model and a given set of parameters to calculate simulated data (called the *model response*), comparing the model response with the values given by the observed data, and then varying the parameters to fit the data more closely. We illustrate this procedure as follows:

1. The model gives a relation between  $m$  parameters  $p_j$ . For each set of values of  $p_j$ , we get a model response  $f(p_1, p_2, p_3, \dots, p_m)$ , which has a value  $f_i(p_1, p_2, p_3, \dots, p_m)$  at each of the  $n$  data points.

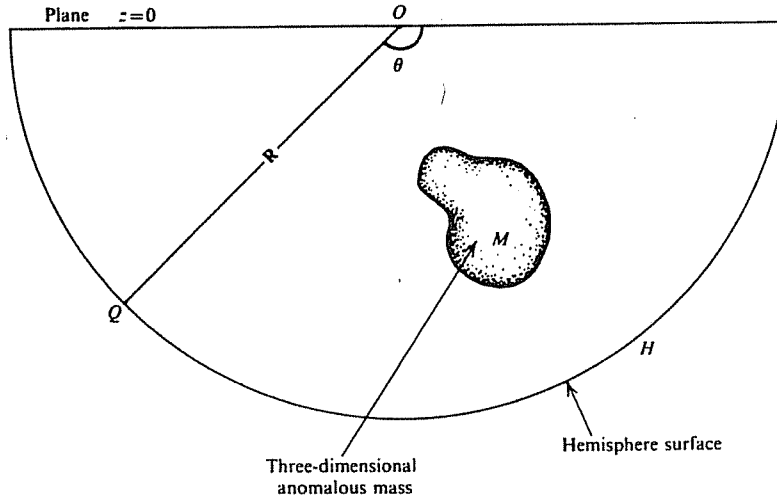


Figure 2.35. Calculation of excess mass.

We write

$$e_i = f_i(p_1, p_2, p_3, \dots, p_m) - c_i \quad i = 1, 2, \dots, n \quad (2.82)$$

where  $c_i$  are the observed data that  $f_i$  are intended to match and  $e_i$  are the errors between the observed data and the model response. We begin with an estimate of  $p_j$ .

2. Because  $f(p_1, p_2, p_3, \dots, p_m)$  generally involves nonlinear relations between the parameters, we simplify calculations by using a first-order Taylor-series expansion to get equations that are linear with respect to the derivatives. Differentiating Equation (2.82), we get

$$\sum (\partial f_i / \partial p_j) \delta p_j = \delta e_i \quad (2.83a)$$

where each derivative is evaluated using the current set of  $p_j$  values. In matrix notation Equation (2.83a) becomes

$$\mathcal{D}\mathcal{P} = \mathcal{E} \quad (2.83b)$$

where  $\mathcal{D}$  is an  $(n \times m)$  matrix whose elements are  $\partial f_i / \partial p_j$ ,  $\mathcal{P}$  is an  $(m \times 1)$  column matrix of the sought-for parameter changes  $\delta p_j$ , and  $\mathcal{E}$  is an  $(n \times 1)$  column matrix whose elements are  $\delta e_i$ .

3. In the usual overdetermined case,  $n \gg m$  and  $\mathcal{D}$  is not square; we use Equation (A.5b) to solve Equation (2.83b):

$$\mathcal{P} = (\mathcal{D}^T \mathcal{D})^{-1} \mathcal{D}^T \mathcal{E} \quad (2.84)$$

This solution is equivalent to  $n$  equations in the

$m$  increments  $\delta p_j$ . Since  $n > m$ , we apply the method of least squares (Sheriff and Geldart, 1983, §10.1.5) to obtain the values of  $\delta p_j$ . The  $p_j$  are then replaced by  $p_j + \delta p_j$  and the calculations are repeated. Iteration is stopped when  $\sum e_i^2$  is smaller than some acceptable (prespecified) value.

Many modifications of the preceding procedure exist, notably methods that stabilize the procedure. If  $\mathcal{D}$  is too large to be efficiently handled by the computer, procedures such as steepest descent or conjugate gradient methods, may be employed. Marquardt (1963) employs an adjustable damping factor, whereas Jackson (1979) and Tarantola and Valette (1982) introduce a priori information to constrain the problem (see §3.8.2, example 3, for a similar magnetic procedure). If the model is highly nonlinear, these methods may not work well and Monte Carlo methods may be appropriate.

## 2.7.10. Excess Mass

Although there is no unique solution to a set of potential field data, it is possible to determine uniquely the total anomalous mass, regardless of its geometrical distribution. Sometimes this is a useful calculation (although potentially dangerous) in estimating ore tonnage in mineral exploration.

To find the *excess mass*, we start with Equation (2.12). Dropping the minus sign, we have

$$\int_S g_n ds = 4\pi\gamma M$$

We surround the mass by a hemisphere whose upper face is the datum plane  $z = 0$ . The surface integral can be separated into two parts: the integral over the

circular base in the  $xy$  plane and the surface of the half-sphere. From Figure 2.35, we have

$$\begin{aligned}\int_S g_n \, ds &= \iint_{z=0} g_n \, dx \, dy \\ &+ \iint_H g_n R^2 \sin \theta \, d\theta \, d\phi = 4\pi\gamma M\end{aligned}$$

where  $g_n$  in the integral over the datum plane  $z = 0$  is the residual anomaly  $g(x, y)$  and  $R$  is the radius of the hemisphere. We take  $R$  large enough that  $M$  is in effect a point mass at the origin and  $g_n = \gamma M/R^2$  at the hemispherical surface. Integration over this surface as  $\phi$  goes from 0 to  $2\pi$  and  $\theta$  from  $\pi/2$  to  $\pi$  leads to the value  $2\pi\gamma M$ , so that

$$\int_{-\infty}^{\infty} \int_{-\infty}^{\infty} g(x, y) \, dx \, dy = 2\pi\gamma M$$

or

$$M = (1/2\pi\gamma) \int_{-\infty}^{\infty} \int_{-\infty}^{\infty} g(x, y) \, dx \, dy \quad (2.85)$$

In practice, the integral is evaluated by numerical integration using the relation

$$M = K \sum g(x, y) \Delta x \Delta y \quad (2.86)$$

where  $m$  is in metric tons or short tons according as  $K = 26.3$  for  $\Delta x, \Delta y$  in meters, or  $K = 2.44$  for  $\Delta x, \Delta y$  in feet. The actual mass producing the anomaly can be determined if we know its density  $\rho_a$  and density contrast  $\Delta\rho$ . This multiplies Equation (2.86) by the factor  $(\rho_a/\Delta\rho)$ :

$$\text{actual mass} = (\rho_a/\Delta\rho) \times \text{excess mass} \quad (2.87)$$

If the regional has not been properly removed, or if other residual anomalies are included, the estimate obviously will be in error.

### 2.7.11. Overburden Effects

In many field situations, the effects of variations in the depth of the overburden may be larger than the effects of different rocks at depth, and so variations in overburden thickness can produce significant gravity anomalies. The average density for an assortment of overburden materials is about  $1.92 \text{ g/cm}^3$  when wet and  $1.55 \text{ g/cm}^3$  when dry, and the averages for wet and dry sedimentary rocks are  $\sim 2.50$  and  $\sim 2.20 \text{ g/cm}^3$ , respectively. Thus a contrast of  $0.6 \text{ g/cm}^3$  is possible.

As a rough estimate, we expect the overburden to be thicker in valleys and low-lying flat land than on steep hillsides and elevated plateaus. Abrupt changes in overburden thickness, however, are common enough. In any gravity survey, and particularly in mineral exploration, it is worthwhile to consider the extent to which gravity anomalies may be caused by variations in overburden thickness.

From the Bouguer correction given in Equation (2.23) and the effect of a semiinfinite horizontal slab, we can get some idea of the magnitude of the overburden effect. The maximum gravity variation that results from a sudden change  $\Delta h$  in overburden thickness, where the density contrast is  $\Delta\rho$ , is given by

$$\Delta g_{\max} = 41.9 \times 10^{-3} \Delta\rho \Delta h \quad (2.88a)$$

$$= 12.8 \times 10^{-3} \Delta\rho \Delta h' \quad (2.88b)$$

where  $\Delta h$  is in meters,  $\Delta h'$  is in feet, and  $\Delta g_{\max}$  is in milligals.

The maximum horizontal gradient of gravity will, of course, be large if overburden irregularity is the source. For abrupt depth changes of 10 m or more in a horizontal distance of 10 m and  $\Delta\rho = 0.6 \text{ g/cm}^3$ , the value of  $(dg_{\max}/dx)$  will be about 0.03 mGal/m. In fact, this steep gradient is more diagnostic than the magnitude of  $g_{\max}$ . Clearly the depth of overburden should be measured in areas of shallow gravity anomalies. This is best done by small-scale refraction or surface resistivity measurements.

### 2.7.12. Maximum-Depth Rules

Smith (1959) gives several formulas for maximum depths of gravity distributions whose shapes are not known, provided that the anomalous bodies have a density contrast with the host rock that is either entirely positive or entirely negative. If  $|g_{\max}|$  and  $|(\partial g/\partial x)_{\max}|$  are the maximum values of gravity and of the horizontal derivative, respectively, the depth to the upper surface has a limiting value given by

$$z \leq 0.86 |g_{\max}| / |(\partial g/\partial x)_{\max}| \quad (2.89)$$

If the anomaly is two dimensional, the factor 0.86 becomes 0.65 in Equation (2.89). However, this expression is not particularly accurate.

## 2.8. FIELD EXAMPLES

- Figure 2.36a shows a Bouguer gravity contour map compiled from a survey in the vicinity of Portland Creek Pond in northern Newfoundland. This was an exploration program for oil and gas in

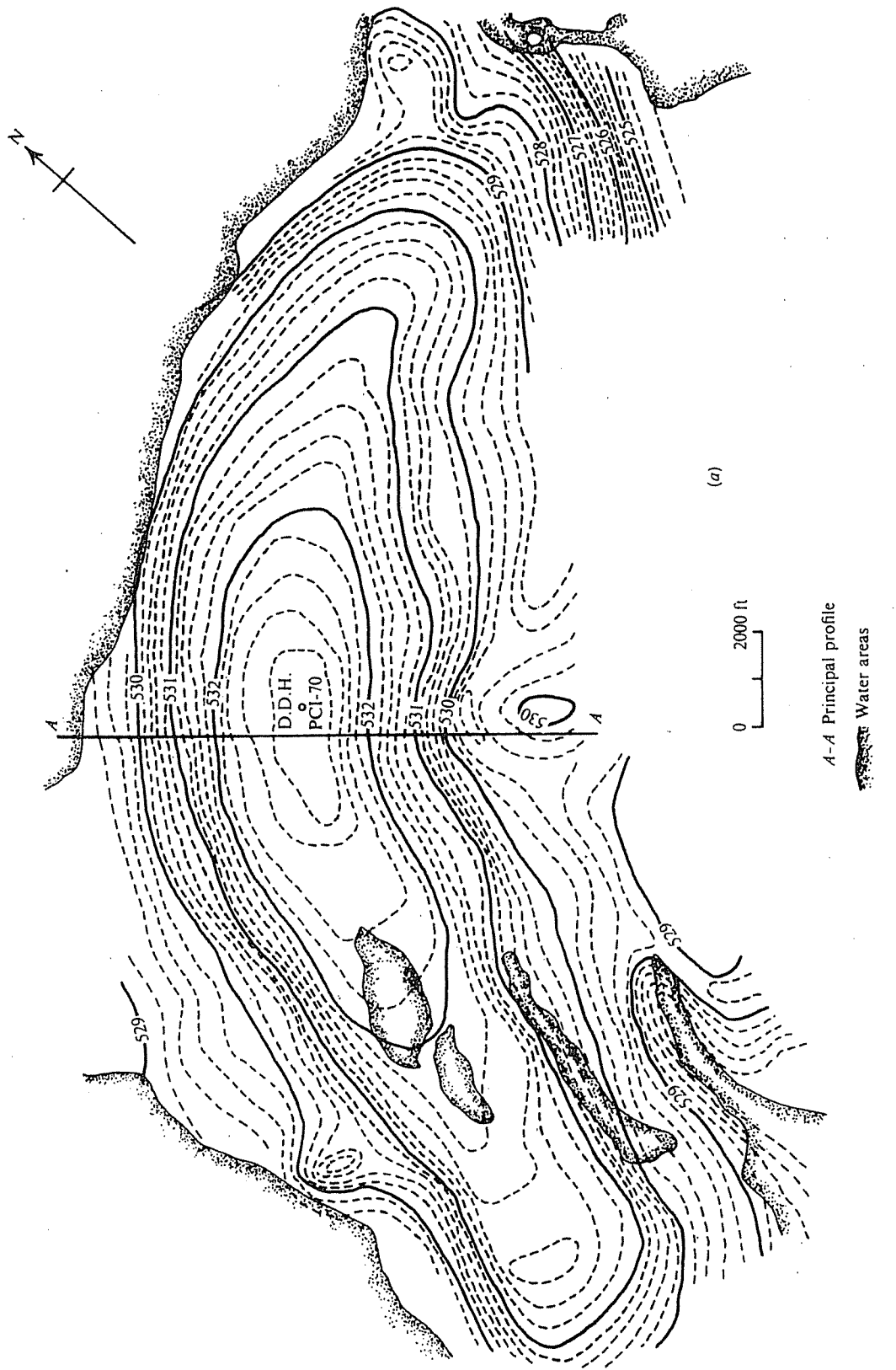


Figure 2.36. Gravity survey, Portland Creek Pond, Newfoundland. (a) Bouguer gravity map, contour interval ( $C_i$ ) = 0.2 mGal.

$A-A$  Principal profile

Water areas

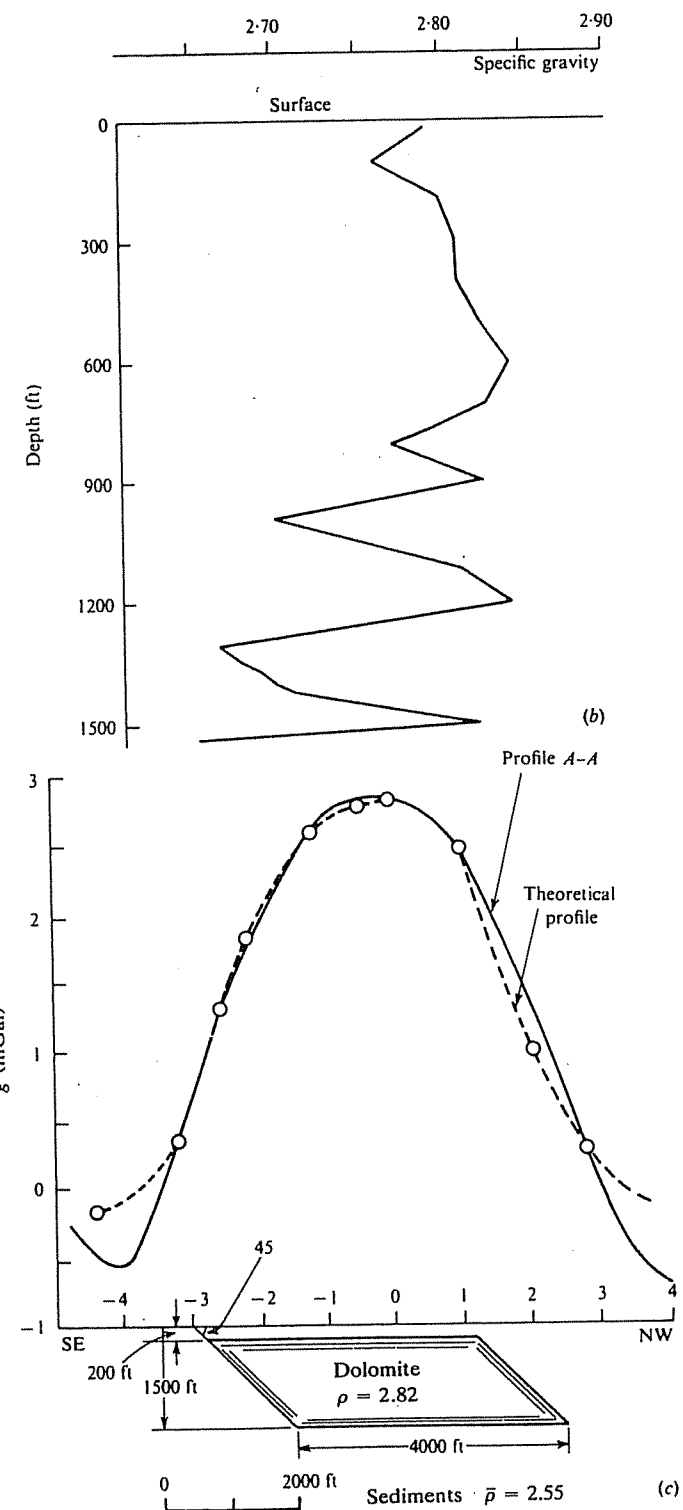


Figure 2.36. (Continued) (b) Density log in borehole DDH PCI-70. (c) Comparison with calculated profile for a 2-D dipping prism.

an area of sedimentary rocks whose thickness, a few miles south, is known to be over 5,000 ft. The topography is reasonably flat and no terrain corrections were required.

It is evident that the large positive anomaly is not a reflection of deep basement structure because the

gradients are too steep. If we use Equation (2.68) to approximate a slab for profile AA' in Figure 2.36a, the values of  $g_{\max}$  and  $(\partial g / \partial x)_{\max}$  indicate that  $h$  is not greater than 650–800 ft. This indicates that the source is shallow and hence must be within the sediments. One possibility is an intrusive dike of

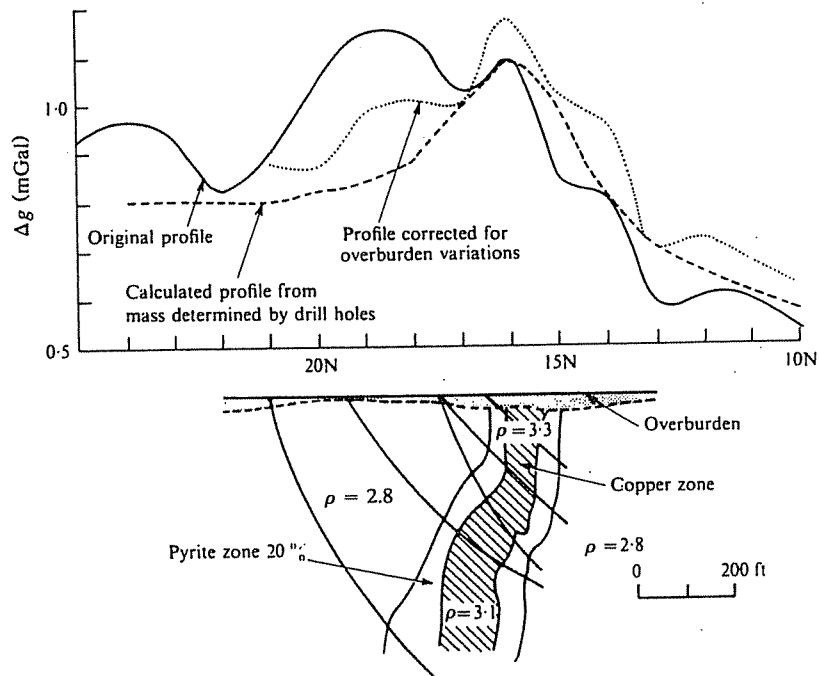


Figure 2.37. Gravity profiles over a copper deposit, Louvicourt, Quebec.

great linear extent, but Equation (2.74) shows that the flanks of the anomaly in this case would be much less steep than the field profile; this suggests that the source is of limited depth.

A 1,600 ft drill hole was put down in the center of this gravity anomaly; its location is shown in Figure 2.36a. Density measurements on core samples at 100 ft intervals are shown in Figure 2.36b. The local presence of dolomite from near surface to 1,000 ft and interbedded with dark shales from 1,000 to 1,600 ft accounts for the positive gravity. The average density of the dolomite samples was 2.82 g/cm<sup>3</sup>. If the surrounding sedimentary formations are assumed to have a density of about 2.55 g/cm<sup>3</sup>, it is possible to match the field profile reasonably well with the dipping prism shown in Figure 2.36c. This analysis is oversimplified since the actual structure is neither two dimensional ( $L \approx 9b$ ) nor homogeneous in the bottom 500 ft. Both factors would steepen the flanks on the profile.

(2) The profiles in Figure 2.37 illustrate the pronounced effect of overburden thickness on gravity results. This is the Louvicourt Township copper deposit near Val d'Or, Quebec. Discovery was made by drilling a weak Turam anomaly (§7.4.3b); the gravity survey was carried out immediately after.

The original Bouguer gravity profile indicated a weak anomaly of 0.15 mGal directly over the conductor and a much broader and larger magnitude anomaly about 75 m to the north. Obviously the small peak would not have aroused any great enthusiasm. Later, when it had been established that the overburden thickness increased appreciably immedi-

ately over the sulfide zone, it was possible to correct for this variable thickness, as discussed in Section 2.7.11, using a density contrast of about 0.08 g/cm<sup>3</sup> between the host rock and the overburden. This is equivalent to 0.03 mGal/m of overburden thickness. In the corrected field profile the larger anomaly to the north has practically disappeared and the small peak has been enhanced to 0.3 mGal. A third profile calculated from density measurements of diamond drill cores is also shown.

This example clearly indicates the importance of measuring the overburden thickness in conjunction with gravity applied to small-scale mineral exploration. This is particularly necessary in surveys for vein-type base-metal deposits that respond to EM methods. The overburden effect would be less pronounced in regions favorable for IP, that is, large-area low-grade disseminated mineralization.

(3) The Delson fault is a well-documented structural feature in the St. Lawrence lowlands. Striking roughly E-W, it is located east of the St. Lawrence River several kilometers southeast of Montreal. Although the area is generally covered by about 15 m of overburden, there are exposures of Utica shales and Chazy limestones in river beds to indicate the location and direction of the fault. The sedimentary beds of the lowlands are flat-lying shales, limestones, and dolomites of Paleozoic age underlain by Precambrian basement rocks at a depth usually greater than 750 m.

Figure 2.38 shows a Bouguer gravity profile taken across the Delson fault in a N-S direction, together with a geologic section. A linear regional trend of

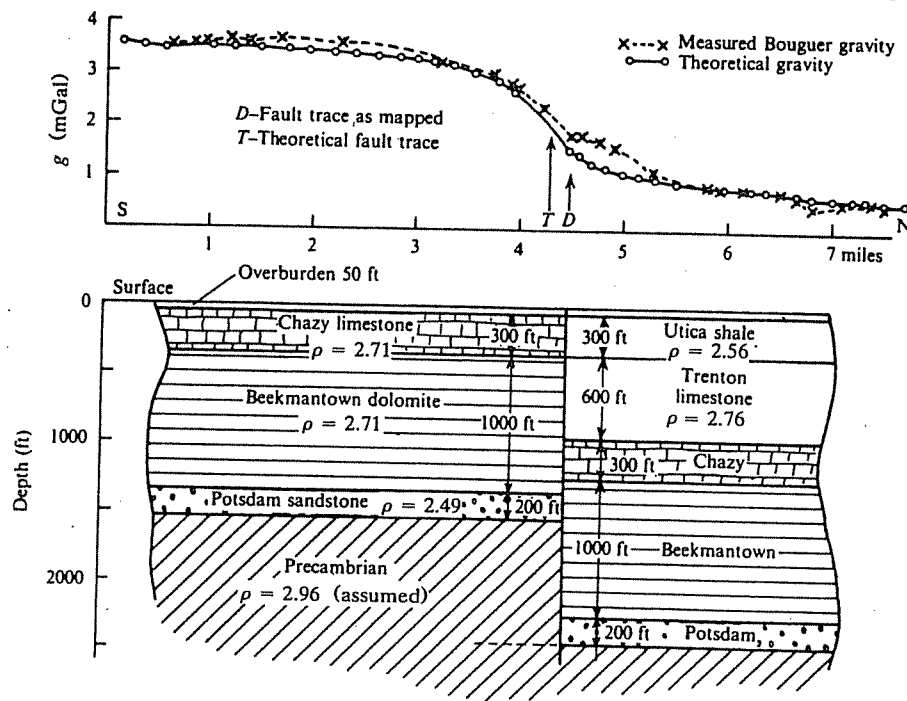


Figure 2.38. Gravity profile and geologic section across the Delson fault, St. Lawrence lowlands.

0.45 mGal/km positive to the south, has been removed.

The profile in Figure 2.38 resembles the gravity effect of a horizontal slab rather than a fault (compare with Figs. 2.28, 2.29, and 2.32). The only appreciable gravity effect from the sedimentary beds would be provided by the juxtaposition of the Chazy and Utica formations near surface and the displaced Potsdam layer (whose thickness is in some doubt) at greater depth. The first pair produces a gravity profile of the proper shape with a total variation of 0.57 mGal and maximum slope of 3.7 mGal/km; thus the total anomaly is too small and the slope too large to fit the field profile. The low-density Potsdam section, on the other hand, would tend to reduce the anomaly, since the bed nearer the surface lies on the south side of the fault; the total effect, however, is only about -0.1 mGal and maximum slope -0.15 mGal/km.

By postulating a density of 2.96 g/cm<sup>3</sup> in the Precambrian rocks and a step of 275 m on the fault down to the south, we obtain a total anomaly of 2.1 mGal with maximum slope of 1.2 mGal/km. The theoretical profile in Figure 2.38 is the result.

The theoretical profile is shifted about 300 m south of the mapped fault location. There are two explanations for this. First, the Delson fault is not vertical, but dips north about 80°. Second, faults very rarely show single clear-cut faces, that is, there is a faulted region of some width. The field profile also shows a small anomaly about 2½ miles north of

the Delson fault, although there is no supporting geological evidence.

## 2.9. PROBLEMS

1. Verify Equation (2.8). [Hint: Start with Equation (2.6a), integrate along the  $y$  axis between the limits  $\pm L$ , and subtract the potential at  $(x^2 + z^2) = a^2 = 1$  (this avoids  $U \rightarrow \infty$  as  $L \rightarrow \infty$ ). By setting  $L = \infty$ , we get Equation (2.8).]
2. Show that Equation (2.12a) holds for an arbitrary closed surface  $S$  regardless of the position of  $m$  within  $S$ . [Hint: Write the integrand in the form  $\gamma m(ds \cos \theta / r^2) = \gamma m d\Omega$ , where  $r$  is the distance from  $m$  to  $ds$ ,  $\theta$  is the angle between  $r$  and  $n$ , the outward-drawn normal to  $ds$ , and  $d\Omega$  is the element of solid angle subtended by  $ds$  at  $m$ . Consider the case where  $r$  cuts  $S$  more than once.]
3. Verify Equations (2.62) and (2.63). [Hint: A solution of Equation (2.11c) is (Pipes and Harvill, 1970, p. 348)]

$$g(r, \theta)$$

$$= 2\pi\gamma\rho \left\{ \sum_{n=0}^{\infty} a_n r^n + \sum_{n=0}^{\infty} b_n r^{-(n+1)} \right\} P_n(\mu)$$

where  $\mu = \cos \theta$ . When  $r > z > R$ , we use the